Biochar

ORIGINAL RESEARCH

Open Access

Relevant biochar characteristics influencing compressive strength of biochar-cement mortars

Julia Hylton[1], Aaron Hugen[1], Steven M. Rowland[2], Michael Griffin[2] and Lori E. Tunstall[1*]

Abstract

To counteract the contribution of CO_2 emissions by cement production and utilization, biochar is being harnessed as a carbon-negative additive in concrete. Increasing the cement replacement and biochar dosage will increase the carbon offset, but there is large variability in methods being used and many researchers report strength decreases at cement replacements beyond 5%. This work presents a reliable method to replace 10% of the cement mass with a vast selection of biochars without decreasing ultimate compressive strength, and in many cases significantly improving it. By carefully quantifying the physical and chemical properties of each biochar used, machine learning algorithms were used to elucidate the three most influential biochar characteristics that control mortar strength: initial saturation percentage, oxygen-to-carbon ratio, and soluble silicon. These results provide additional research avenues for utilizing several potential biomass waste streams to increase the biochar dosage in cement mixes without decreasing mechanical properties.

Highlights

- A broad selection of biochars were used to replace 10 wt.% cement in mortars, resulting in similar or improved strength.
- Biochar moisture saturation percentage, O/C, and soluble silicon are the most important predictors of mortar strength.
- The data support the hypothesis that biochar improves strength via internal curing, found to be the most important mechanism.

Keywords Biochar, Concrete, Compressive strength, Predictor variables, Multivariate linear model

*Correspondence:
Lori E. Tunstall
ltunstall@mines.edu
Full list of author information is available at the end of the article

Graphical Abstract

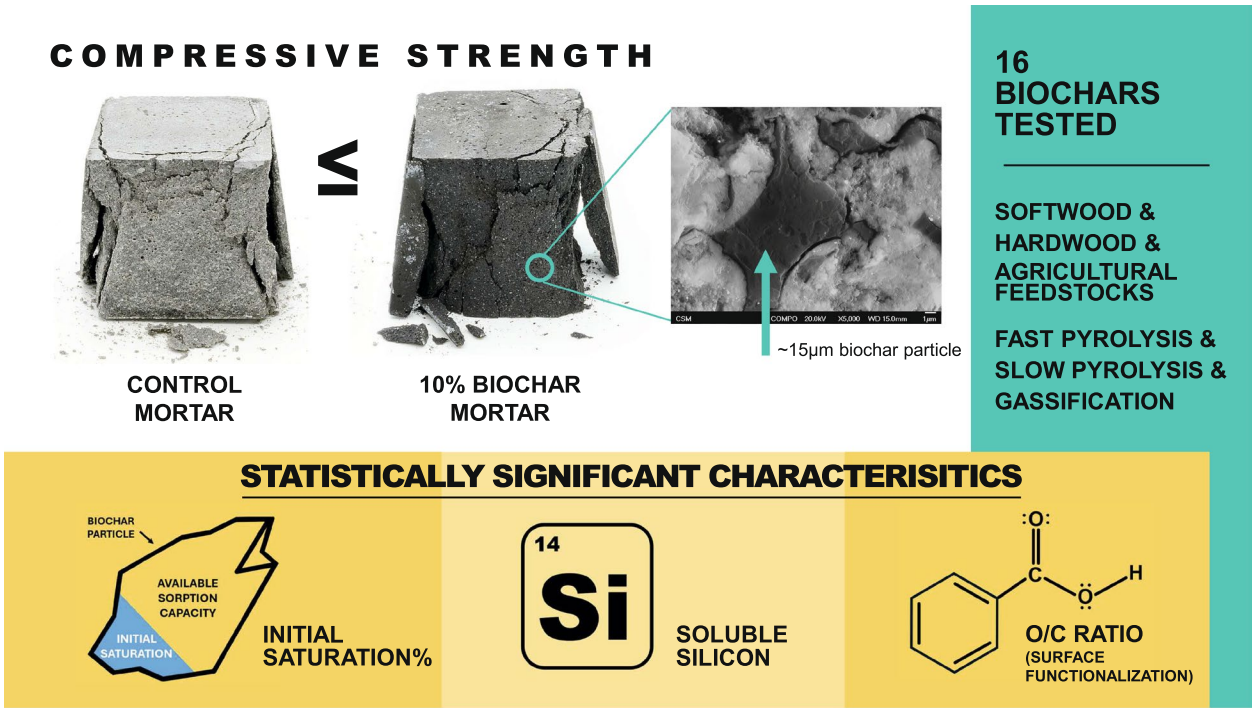

1 Introduction

To reduce global temperatures to preindustrial levels as per the Paris Agreement, CO_2 emissions must be drastically reduced. Concrete manufacturing and utilization is responsible for ~ 8% of all anthropogenic CO_2 emissions (Busch et al. 2022; Wang et al. 2023; Nehdi et al. 2024). As the urgency to reduce emissions increases, the cement industry is looking for low-cost, high-quality alternatives to reduce their carbon footprint. Over the last decade, biochar has emerged as a competitive option to reduce embodied carbon in cement structures. Biochar, a carbon-rich material made from biomass feedstock, has been shown at lab scale to integrate into concrete as a partial cement replacement without reducing concrete's compressive strength at low dosages (Maljaee et al. 2021; Aman et al. 2022; Liu et al. 2022; Chen et al. 2023; Kamini et al. 2023; Lin et al. 2023; Senadheera et al. 2023; Zhang et al. 2023; Barbhuiya et al. 2024; Murali and Wong 2024; Zaid et al. 2024). However, at cement replacements above 2–5 wt.%, strength decreases are typically observed. In contrast, with a careful mix design and some preparation of the biochar, our lab has observed similar or improved strengths using 16 different biochars at a 10% cement replacement level by mass. This work investigates why some biochars perform more favorably than others, using machine learning approaches and statistical analysis to elucidate the relevant physical and chemical biochar characteristics for improved compressive strength in the cement mortars studied. The end goal is to identify key characteristics for producing or selecting biochar suitable for high cement replacement levels in concrete. Since there is a direct relationship between the quantity of biochar used as a cement replacement and the quantity of CO_2 offset, the target is to increase the biochar dosage as much as possible without sacrificing the concrete's engineering properties.

1.1 Biochar background

1.1.1 Carbon sequestration potential

Biochar is a waste product made from the thermal decomposition of biomass in an oxygen limited environment, a method known as pyrolysis. By limiting the oxygen availability, the aromatic carbon in the biomass does not combust and instead is formed into a decomposition-resistant structure. During the pyrolysis process, recalcitrant carbon structures form highly condensed, or aromatic, structures that are converted through radical reactions to produce the final biochar. The conversion to biochar keeps the carbon from oxidizing into carbon dioxide, as the biomass would do without intervention; in

fact, this structure can resist decomposition for hundreds to thousands of years (Ippolito et al. 2020). By limiting the potential for biomass to decompose and emit CO_2 into the atmosphere, the stable carbon in biochar can be added to concrete as a carbon sink.

Most of the CO_2 emissions from the concrete industry are from the production of cement powder, the active ingredient in concrete. The main component in cement, CaO, requires high temperature calcination of limestone, $CaCO_3$. This process is responsible for 60–65% of all the CO_2 emissions associated with concrete (Nehdi et al. 2024); the remaining emissions are associated with electricity usage and transportation. According to the Environmental Product Declaration for Portland Cement for 2021–2026, one kg of cement production produces 0.92 kg of $CO_{2,eq}$ (PCA 2021). By replacing some of the cement used in concrete with a carbon-negative material like biochar, it is possible to significantly offset a portion of the CO_2 emitted during manufacturing. Since ~ 2.2 kg of CO_2 is sequestered in 1 kg of biochar (Delaney and Hawkes 2011), replacing 1 kg of cement with biochar results in ~ 3.12 kg CO_2 avoided/sequestered; however, it is possible that this estimate is high or low for some of the biochars used, since the true carbon sequestration potential of biochar depends on many factors, including feedstock sourcing, pyrolysis conditions, fixed carbon percentage, trucking, etc., which were not evaluated as part of this work. Moreover, biochar cementitious composites also require additional superplasticizer, which has a global warming potential of 1.5 kg of $CO_{2,eq}$ per kg of additive (EPD 2023). Nevertheless, the sequestration capacity of biochar far outranks any other partial cement replacement (such as fly ash, blast furnace slag, and natural pozzolans) that only reduces emissions by reducing the cement quantity used.

This study used a mix design in which 10% of the cement mass was replaced with biochar, offsetting the overall carbon footprint by an estimated 32% compared to the same mix without any biochar. This carbon footprint estimate considers both cement replacement with biochar and the additional superplasticizer required to achieve comparable flow (an estimated ~ 10x increase compared to a control mix).

1.1.2 Pyrolysis methods

Pyrolysis is the thermal decomposition of a biomass (typically agriculture waste, forest residue, or other abundant plant matter) in a limited oxygen environment which produces bio-oil, pyrolysis gas, and biochar. In contrast to combustion, pyrolysis typically occurs under an inert nitrogen atmosphere with little to no oxygen available. Figure 1 shows how pyrolysis locks the carbon in biochar rather than releasing oxidized carbon into the atmosphere as CO_2. By preventing the carbon-rich biomass from oxidizing, either during high heat combustion or over time during natural decomposition, pyrolysis produces a decomposition-resistant form of carbon, sequestering carbon that would otherwise be emitted into the environment, either as CO_2 or CH_4. Additionally, by integrating biochar into concrete as a carbon sink, the embodied carbon emission from the concrete production can be partially sequestered into the final building material.

Depending on the pyrolysis heating conditions, the ratios of the final products (biochar, bio-oil, and pyrolysis gas) can vary drastically, summarized in Table 1. In the

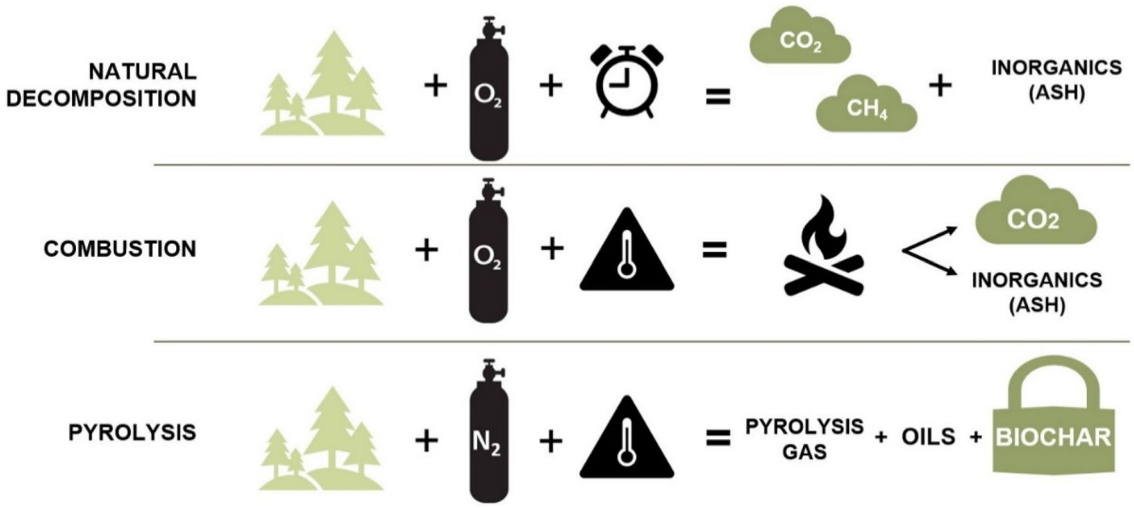

Fig. 1 Graphic comparison of thermochemical conversions of biomass exposed to various environments and the resulting byproducts. Green graphics represent the main carbon products

Table 1 Comparison of pyrolysis methods used in this study—modified from (Igalavithana et al. 2017; Tomczyk et al. 2020)

	Slow pyrolysis	Fast pyrolysis	Gasification
Temperature range (℃)	350–800	400–800	700–1500
Heating rate (℃min^{-1})	< 10	~ 10,000	~ 100
Residence time	Minutes-hours	Seconds	Seconds-minutes
Biochar yield	~ 35%	~ 10%	~ 10%
Bio-oil yield	~ 30%	~ 70%	~ 5%
Pyrolysis gas yield	~ 35%	~ 20%	~ 85%
Typical application	Soil remediation	Biofuel production	Gas/fuel production

current market, biochar is largely used in soil remediation from a slow pyrolysis process that has a high biochar yield. In the renewable energy sector, fast pyrolysis is a promising pathway to produce bio-oil for fuel applications, while the low percentage of biochar produced as a byproduct is underutilized. Repurposing the biochar waste from the biofuel industry has the potential to reduce market barriers for biofuel adoption through decreased cost, which can further reduce global CO_2 emissions (Wright et al. 2010).

Pyrolysis conditions are the most general way to classify biochars as the production techniques dictate several of the biochar's final characteristics. For instance, in slow pyrolysis there is a two-step decomposition process where the pyrolysis gas is released and then the carbon body softens, collapses, and condenses while the carbon structure polymerizes (Qin et al. 2022). With fast pyrolysis, when the biomass decomposes, the softening and condensing happens simultaneously; the pyrolysis gas escapes quickly through the softened carbon matrix of the biomass, significantly increasing the surface area of the final biochar (Newalkar et al. 2014). While these comparisons are reliable for the processing of a particular feedstock group, the feedstock itself also has a considerable impact on the final chemical and physical properties of the biochar (Ippolito et al. 2020).

This work primarily aims to elucidate the structure–property relationship between biochar and mortar strength; however, it will also discuss the general pyrolysis process parameters that can affect the key biochar characteristics.

1.2 Biochar concrete background

The complexity and variability of biochar makes it difficult to compare published studies on biochar concrete. Many works do not report the feedstock type or pyrolysis conditions of the biochar used nor the laboratory preparation methods. This is problematic since there is not yet a consensus on the relevant parameters controlling successful integration of biochar into concrete, resulting in variable outcomes and conclusions. This study aims to experimentally determine what biochar characteristics impact compressive strength through assessment of 16 distinct biochars as cement replacements in mortars. By understanding the important characteristics of biochar for concrete integration, those properties can be controlled to increase the biochar dosage and thus the global CO_2 offset. Moreover, it will provide a useful guideline for which biochar characteristics should be reported in future research. Figure 2 is taken from a thorough review highlighting the importance of biochar characterization on understanding final composite properties (Maljaee et al. 2021). Almost all the column III properties were quantified in this study, as well as additional characteristics, to systematically investigate possible factors influencing strength development in biochar-cement composites.

There are several recent reviews on biochar concrete studies (Maljaee et al. 2021; Aman et al. 2022; Kamini et al. 2023; Senadheera et al. 2023; Zaid et al. 2024; Zhao et al. 2024) that all strongly recommend a maximum cement replacement with biochar below 5%. However, our research laboratory consistently achieves comparable or improved mortar strength cement replacement level up to 15%. The methodology that makes this possible is patent pending (Pecha et al. 2022). The contradiction between these reviews and our results emphasize that more research is needed to understand the important parameters behind strength development in these composite mixes. Due to material quantity limitations from some suppliers, a 10% biochar dosage was chosen for this work so that mortars could be compared at the same percentage of biochar. A 10% biochar dosage was preferable to the widely recommended 5% for two primary reasons: (1) to demonstrate that a broad range of biochar feedstocks and pyrolysis conditions can be used to sequester a significant amount of CO_2 without sacrificing mortar strength; and (2) to exaggerate the effects of each biochar's physical and chemical characteristics so that key control variables could be identified.

Though there is no shortage of studies on biochar mortar behavior, there is a general knowledge gap on the specific biochar properties that dictate those behaviors. The

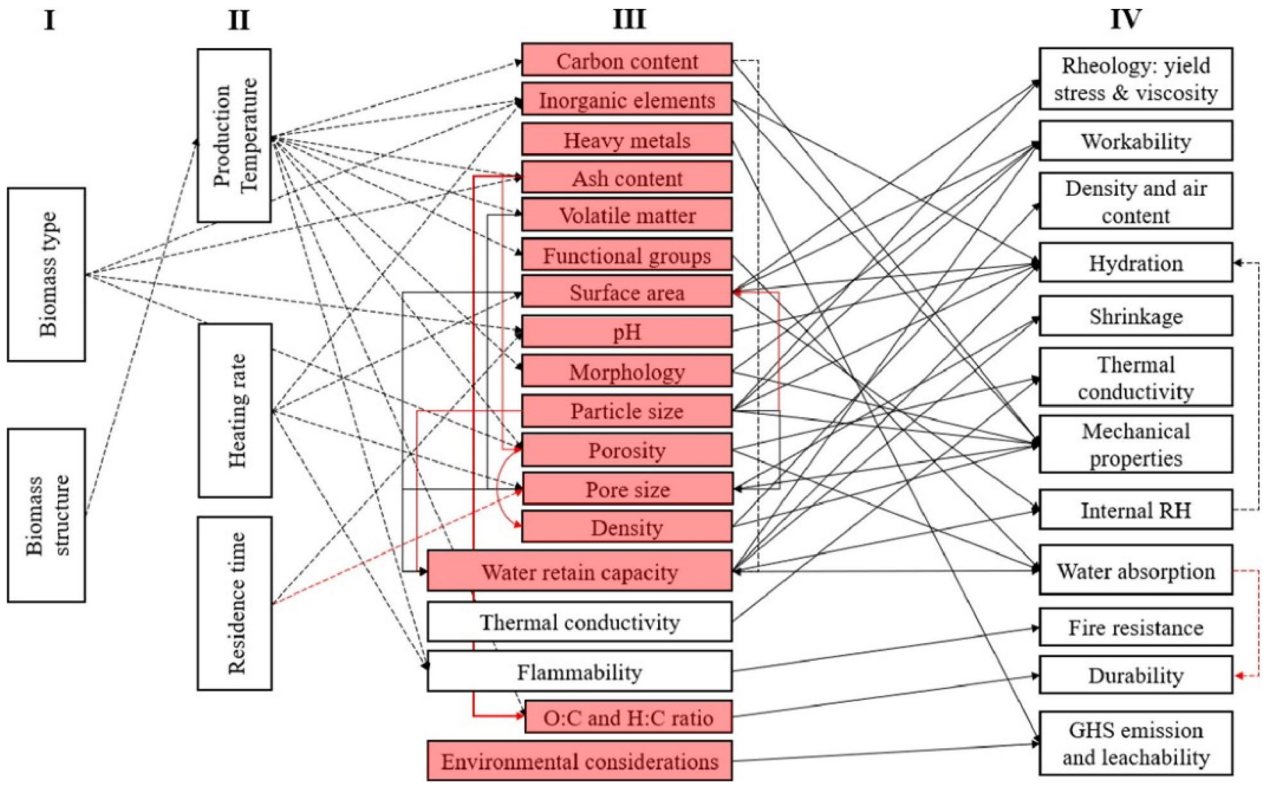

Fig. 2 A map showing how biomass factors (I) influence pyrolysis parameters (II) which dictate biochar properties (III) and ultimately cement composite properties (IV) where red lines indicate inverse effects. The red sections in column III indicate all the characteristics quantified in this study. Reprinted from (Maljaee et al. 2021) with permission from Elsevier

two prevailing hypotheses describing why a small dosage of biochar can be beneficial for composite compressive strength are: (*H1*) internal curing; and (*H2*) filler effect.

Hypothesis 1 Biochar has a high liquid adsorption capacity which encourages the material to act as an internal curing agent, collecting much of the mix water during cement mixing and lowering the effective water to cement ratio during concrete hardening. Then during the curing process, a humidity gradient occurs between the biochar particles and the densifying cement matrix, causing the adsorbed water to be slowly released and internally cure/hydrate the surrounding matrix, ultimately increasing the compressive strength (Gupta and Kua 2018, 2019; Maljaee et al. 2021; Zhang et al. 2022; Chen et al. 2023; Kamini et al. 2023; Kua and Tan 2023; Senadheera et al. 2023; Barbhuiya et al. 2024; Murali and Wong 2024; Zaid et al. 2024).

Hypothesis 2 Biochar is less dense than cement powder so replacing a mass percentage of the cement powder with biochar increases the volume of particles in the mix, while decreasing the interparticle spacing. This increased volume of insoluble, high-surface-area particles provides additional surface area for the nucleation and growth of cement hydration products, thus densifying the cement matrix and ultimately increasing the final composite's compressive strength (Tan et al. 2021; Liu et al. 2022; Barbhuiya et al. 2024; Murali and Wong 2024; Zaid et al. 2024).

This work assesses 16 distinct biochars as partial cement replacements in mortars, using machine learning to evaluate these hypotheses using multivariate correlations between various biochar characteristics and mortar strength. To our knowledge, this is the first time a study has statistically evaluated correlations between mortar strength and chemical and physical properties of numerous industrially produced biochars. This analysis allows us to assess the validity of existing hypotheses while also illuminating new correlations not previously considered.

2 Materials

2.1 Biochars

2.1.1 Pyrolysis and milling

Biochars that are produced commercially from a variety of vendors and feedstocks were used in this study to cover a wide range of production parameters that are currently

relevant to the biochar market. The biochar samples are organized and named according to general feedstock and pyrolysis conditions, since these parameters dictate many of the main differences among biochars (Igalavithana et al. 2017). Table 2 lists the samples and naming conventions used in this study. Feedstocks are categorized as

Table 2 Biochar samples and pyrolysis conditions used in this study

Biochar sample name	Feedstock material	Feedstock category	Pyrolysis type	Temperature [°C]
SW.FP.01	Forestry residue	Softwood	Fast	760
SW.FP.02	Forestry residue	Softwood	Fast	500
SW.FP.03	Forestry residue	Softwood	Fast	500
SW.FP.04	Pine	Softwood	Fast	500
SW.FP.05	Pine	Softwood	Fast	500
SW.SP.01	Southern yellow pine	Softwood	Slow	700
SW.SP.02	Mixed pine	Softwood	Slow	700
SW.SP.03	Western pine	Softwood	Slow	700
HW.FP.01	White hardwood	Hardwood	Fast	500
HW.FP.02	Poplar	Hardwood	Fast	500
HW.SP.01	Aspen	Hardwood	Slow	400
HW.SP.02	White hardwood	Hardwood	Slow	500
AG.G.01	Pistachio shells	Agricultural	Gasification	1100
AG.SP.01	Rice hulls	Agricultural	Slow	450
AG.SP.02	Walnut shells	Agricultural	Slow	800
AG.SP.03	Olive pits	Agricultural	Slow	800

Table 3 Oxide composition of the OPC used in this study, measured by XRF

	SiO_2 [wt.%]	Al_2O_3 [wt.%]	Fe_2O_3 [wt.%]	CaO [wt.%]	MgO [wt.%]	SO_3 [wt.%]	Na_2O [wt.%]	K_2O [wt.%]	P_2O_5 [wt.%]	TiO_2 [wt.%]
OPC	19.34	4.12	3.29	62.96	0.75	3.01	0.17	0.84	0.10	0.17

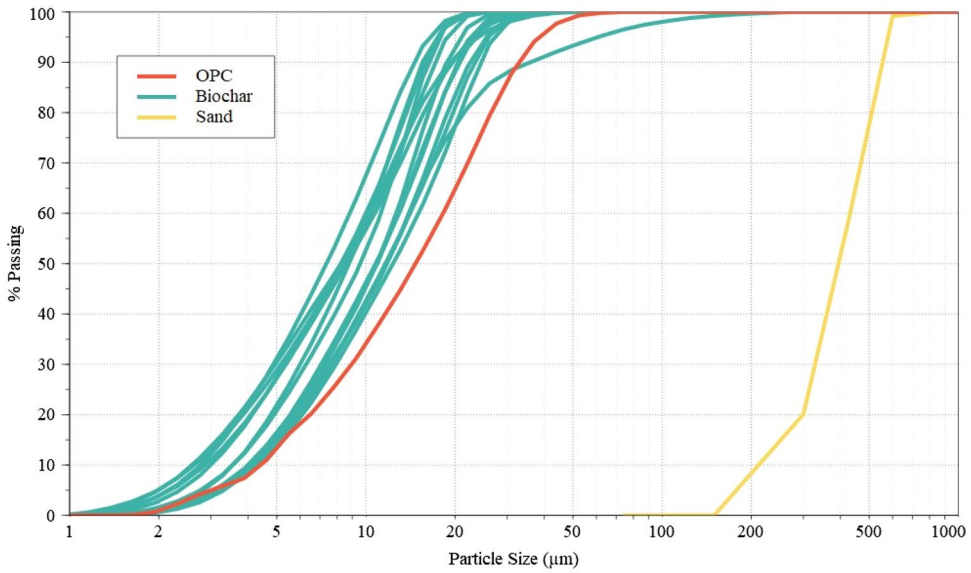

Fig. 3 Particle size distribution of dry materials used in cement mortar mixes

softwood (SW), hardwood (HW), and agricultural (AG); pyrolysis conditions are categorized as fast (FP), slow (SP), and gasification (G).

After pyrolysis, the biochar particles were dry milled in a RockLabs Standard Ring Mill for 3–4 min in 250–350 g batches. The biochar was milled below its macropore level (20 µm) to allow for more successful integration into the mortar. Unmilled biochar retains the cellular pore structure of biomass, and thus is brittle, resulting in decreased compressive strength cementitious composites (Dixit et al. 2019). Integrating unmilled biochar that retains its macroporosity has been shown to negatively impact compressive strength as the macroporosity creates a preferential fracture path outside of the cement matrix. However, because the macroporosity makes the unmilled biochar fragile, milling to the correct particle size takes minimal time.

2.2 Mortar materials

All mortar samples were made using the same Type I/II ordinary Portland cement (OPC) powder from Holcim and Ottawa test sand sourced from Humboldt, conforming to ASTM C150 and C778, respectively (ASTM C150 2000; ASTM C778 2000). The XRF oxide composition of the cement used in this trial is shown in Table 3. Particle size distributions of dry materials are shown in Fig. 3; after milling, all the biochars had an average particle size (d50) below the sand and cement. Each mix design uses a liquid high-range water reducer (Sika® ViscoCrete®-2100), hereafter referred to as superplasticizer, or SP. Mix water was unfiltered tap water.

3 Methods

3.1 Mix design

The mortar mix designs used in this study are detailed in Table 4. For samples containing biochar, 10% of the cement mass was replaced with an equal mass of biochar, as shown in Fig. 4. The mix design uses a water-to-cement (w/c) mass ratio of 0.45. Note that for the mixes containing biochar, the w/c is kept at 0.45 though less cement is used. In other words, the biochar is not considered to be cementitious, so the biochar mixes use slightly less water overall. Since the biochars all hold some water under ambient conditions, the initial moisture content of each biochar was measured and subtracted from the total mix water added. While an argument can be made that observed strength increases may be due to using less water, since there is no definitive evidence that the biochar is cementitious, we conclude that the most appropriate control is to maintain the same w/c (not the same total water added).

Each biochar mix produced 12 50-mm mortar cubes conforming to ASTM C109 (C109 2016). All mixing was done in a 5Q KitchenAid mixer with the whisk attachment on speed 4–6. The dry ingredients were added first (sand, cement, and biochar) and dry mixed until visually homogeneous (~ 5 min). Then 90% of the mix water was added slowly while mixing, while the

Table 4 Mix designs for the biochar cement mortars

Mix	Biochar Density [g cm^{-3}]	Biochar initial moisture [wt.%]	Cement [g]	Sand [g]	Biochar [g]	Water [g]	SP:cement [wt.%]	Wet mix flow [%]
Control	–	–	1000	2230	0	450.0	0.01	108
SW.FP.01	1.95	1.21	900	2230	100	403.8	1.01	128
SW.FP.02	1.87	2.84	900	2230	100	402.2	0.78	116
SW.FP.03	1.81	1.50	900	2230	100	403.5	0.80	115
SW.FP.04	1.69	2.57	900	2230	100	402.4	0.78	124
SW.FP.05	1.58	2.76	900	2230	100	402.2	1.34	120
SW.SP.01	1.40	3.15	900	2230	100	401.9	1.19	136
SW.SP.02	2.68	4.95	900	2230	100	400.1	0.44	107
SW.SP.03	2.28	3.73	900	2230	100	401.3	0.88	128
HW.FP.01	1.65	1.67	900	2230	100	403.3	1.12	110
HW.FP.02	1.89	2.94	900	2230	100	402.1	0.78	104
HW.SP.01	1.55	2.13	900	2230	100	402.9	2.78	99
HW.SP.02	2.08	1.37	900	2230	100	403.6	0.84	112
AG.G.01	1.94	6.25	900	2230	100	398.8	1.20	97
AG.SP.01	1.73	5.69	900	2230	100	399.3	1.12	140
AG.SP.02	1.75	13.40	900	2230	100	391.6	0.65	100
AG.SP.03	1.88	13.70	900	2230	100	391.3	0.64	96

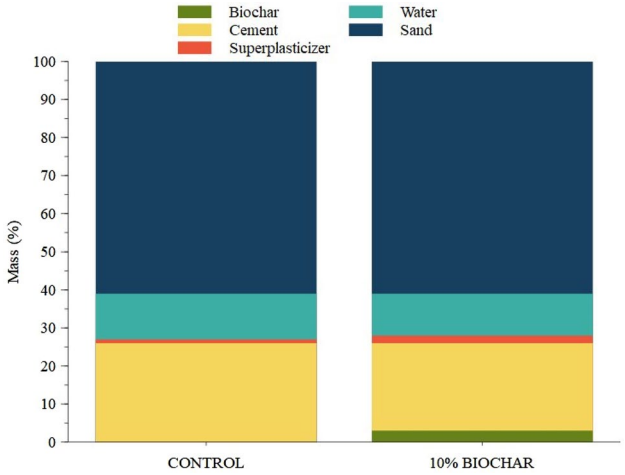

Fig. 4 Mass contribution of each component in the mortar mixes

remaining 10% of the water was first mixed with SP then added slowly to the mixing bowl. The addition of water triggered the start of the mix time, which was 2–4 min for all mixes. All 16 biochars exhibited high water demand and thus greatly reduced the flowability of the mortar mix; this stiffness was corrected with the use of a high range superplasticizer. Compared to the control mortar, a high dosage of superplasticizer is needed to achieve a similar flow with the addition of biochar. Decreased flow is a well-documented challenge with biochar cementitious composites and has been more thoroughly investigated in other works (Gupta and Kua 2019; Arowojolu et al. 2023; Suarez-riera et al. 2024).

The flowability of each mix was tested and additional SP was added if the mix fell below the 105–115% ideal spread for mortars, outlined in ASTM C1473 (ASTM C1437 2009). Briefly, the flow was determined as the % spread of the wet mix after filling a standard volume cone on a drop table; a standardized cone was filled in two lifts with wet mix and removed, then the table was dropped 25 times before the final spread was measured and compared to the initial cone diameter; the flow was reported as a percentage increase from initial to final spread diameter and was recorded within 5 min after mixing. The SP dosage normalized by the cement mass is shown in Table 4. Finally, the mortars were cast into the cubic molds per ASTMC109 and cured in a sealed environment for 24 h (ASTM C1437 2009; C109 2016). The cubes were then demolded and cured in a saturated limewater bath until testing age.

3.2 Compressive strength testing

The cubes were removed from the limewater bath in batches of 3 for compressive strength testing. Each mix was tested at 3, 7, 14, and 28 days of curing but all ages mirrored the trends observed at 28 days of curing so only the final testing age was reported in this work. After curing, the cubes were surface dried and tested for unconfined compressive strength in a Forney F-450-VFD using a load rate of 50 psi/second (0.34 MPa/second) (C109 2016). The maximum stress at break was recorded for each of the three samples and averaged.

3.3 Biochar characterization: physical properties

3.3.1 Density

The skeletal density of the milled biochars was measured using the Micromeritics AccuPyc II with helium gas as the displacement medium. The density measurement was conducted by averaging five cycles of pressurized inlet gas into a known volume and sample mass. The biochar was not dried prior to analysis. Results are included in the mix information in Table 4.

3.3.2 Initial moisture content

Each biochar used in this study was stored in snap-close buckets from the time of milling until use. These containers allowed some exposure to the ambient atmosphere, resulting in some initial moisture content in the biochars. Because the water-to-cement ratio is of such high importance for comparing strength development in cementitious systems, the initial moisture content of the biochars was measured and accounted for in the mortar mix designs. Using the PerkinElmer TGA 8000, 5–20 mg of ambiently stored biochar was run under a nitrogen gas flow and heated to 105 ℃ at 10 ℃ $^{-1}$ min and isothermally held until the weight stabilized, typically under 30 min. The mass loss was assumed to be 100% water vapor and used as the initial moisture content.

3.3.3 CO_2 surface area/pore size distribution

An ASAP 2020 Plus by Micromeritics was used to measure the BET surface area and average pore size of each biochar sample. Roughly 2–4 g of biochar was degassed

Table 5 Compounds and concentrations used to create the simulated cement pore solution

Compound	Concentration [M]
KOH	0.1062
Na_2SO_4	0.0489
K_2SO_4	0.0370
$Ca(OH)_2$	0.0212

at 100 ℃ and then transferred to the analysis port. CO_2 was used as the analysis gas, since it has been shown to give more reliable results than N_2 for highly microporous materials like biochar (Sigmund et al. 2017; Marshall et al. 2019; Maziarka et al. 2021). The sample tube was submerged in an ice bath during analysis where relative pressure was measured at 40 adsorption and 5 desorption points, with maximum P/P° of 0.035.

3.3.4 Particle size distribution

Using a Microtrac S3500 laser particle size analyzer with isopropanol as the solvent, the particle size distribution (PSD) for each biochar sample was measured in triplicate after milling and then averaged. The refractive index of each biochar sample was set to 2.42 (Marshall et al. 2019).

3.3.5 Simulated cement pore solution

To model how the biochar samples interact in a cement system, a simulated cement pore solution was utilized (Tunstall et al. 2017). This solution was used in the liquid sorption capacity experiments as well as the soluble product washes (3.3.6. and 3.3.7.). Table 5 describes the compounds used to produce the simulated cement pore solution.

3.3.6 Liquid sorption capacity (maximum sorption capacity)

To measure the maximum sorption capacity of each milled biochar sample, 1 g of biochar was submerged in 10 g of liquid (tested with both DI water and simulated cement pore solution) in a closed container. The biochar remained in solution for at least 24 h to allow the biochar to fully adsorb. This specific study did not focus on the kinetics or rate of sorption; instead, it modeled an extreme case to compare the maximum liquid sorption capacity for each biochar. It has been shown in other studies that 24 h is ample time for the biochars to fully saturate and low variability was confirmed (Chemerys and Baltrėnaitė 2017; Mechtcherine et al. 2018; Usevičiūtė 2020). After full saturation, the biochars were vacuum filtered through a prewetted 1-µm filter in a Buchner funnel for 5–10 s or until the standing water was removed and the matte black surface of the saturated biochar was exposed. A 10–30 mg sample was quickly collected from the filter paper for analysis with TGA under N_2 flow at 105 ℃ until the mass stabilized (~ 30 min). The mass loss measured from drying the fully saturated biochar includes the loss of the initial moisture present in the biochar prior to full saturation, so the total mass loss is used to calculate the maximum sorption capacity, which is the sum of the initial moisture and the liquid uptake potential.

The percentage mass loss from the TGA was divided by the residual mass percent, resulting in the maximum liquid sorption capacity. In other words, the total evaporated water mass was compared to the final dry biochar mass, demonstrating how much liquid (g/g) the dry biochar can hold. The initial saturation percentage of each biochar was determined by taking the ratio between each biochar's initial moisture content from the total sorption capacity. This metric compares the liquid uptake potential of the biochar once integrated into a mix, since it considers both the total sorption capacity and the percentage already occupied by initial moisture. Equation 1 describes the initial saturation of the biochar as a function of its total sorption capacity.

$$initial\ saturation(\%) = \frac{initial\ moisture\ content(\%)}{total\ liquid\ sorption\ capacity(\%)} \quad (1)$$

Though only one round of saturation testing was conducted for each char, previous laboratory trials indicate that the method is reproducible if the following precautions are taken; the sample must not be over-dried prior to vacuum filtration and the time between vacuum drying and TGA analysis should be minimized. This test was repeated with the same process for biochars exposed to the simulated cement pore solution. DI water was used for final initial saturation calculations because the biochar chemically interacted with the cement pore solution, which will be discussed further in 4.2.3.

3.3.7 Solution wash+ICP-AES analysis of filtrate

To investigate the soluble ions in each biochar, a 1 g sample of biochar was mixed with 100 g of DI water for 18 h, stirred continuously. The biochar was then filtered out and a sample of the leachate was collected through a 0.45-µm filter, diluted twice and analyzed with a PerkinElmer ICP-AES machine. The elemental content report showed the elemental concentration that had leached into the DI water during the biochar's exposure. Each submitted sample was tested in triplicate and the average soluble ion concentration was reported. However, only a portion of the results were reported with relative standard deviation values.

It is important to note that ICP-AES of solutions is most appropriate for quantifying the soluble cations. Soluble anions are typically oxyanions (hydroxyl, carbonate, bicarbonate, sulfate, phosphate, etc.) and cannot be accurately captured by ICP, since it does not measure oxygen concentrations (Fidel et al. 2017). The reported sulfur and phosphorus concentrations were assumed to be in the form of sulfate and phosphate, respectively. The leachates were assumed to be at ionic equilibrium and the missing anion charge is assumed to be undetected oxyanions (Fidel et al. 2017). The alkalinity contributions in biochar are feedstock dependent but total alkalinity has

been shown to be highly correlated with soluble cation concentrations (Fidel et al. 2017). Cations with relevant concentration changes are aluminum, calcium, potassium, magnesium, and sodium. Anions include sulfur and phosphorus assumed to be in the form of sulfate and phosphate. Silicon was not included in the cation or anion categories but was added to the total dissolved mass.

This process was repeated with a simulated cement pore solution instead of DI water. Due to the cement pore solution, these samples had a higher ion concentration and had to be diluted an additional three times. A "blank" filtered pore solution was analyzed via ICP-AES and was used as the baseline, which was subtracted from the biochar-cement pore solution leachate. This resulted in a report of the ionic changes due to each biochar exposure. Negative concentrations indicate concentration consumed from the simulated cement pore solution by the biochar sample, while positive concentrations indicate ions present in excess of those found in the cement pore solution.

3.3.8 Shear rate and filler effect

In cement mixes, a filler effect refers to an inert material that potentially increases both the rate of the anhydrous cement particle dissolution due to increased shearing and the nucleation of hydration product due to additional surface area (Berodier and Scrivener 2014). To investigate whether biochar particles contribute a filler effect in mortar mixes, the interparticle shear rate and particle spacing were calculated. These values give an indication of the filler effect (Berodier and Scrivener 2014). Using the mix proportions (M_{cement} and $M_{biochar}$), the surface area of the dry ingredients (BET_{cement} and $BET_{biochar}$), the density of the final mix (ρ), and the particle size distributions ($d10$ and $d95$ of all dry materials), Eqs. 2 and 3 calculate the average distance between the surface of particles during mixing (δ). The relative packing fraction ($\frac{\phi}{\varphi_m}$) uses the solid volume of the mix (ϕ) and the maximum packing fraction (ϕ_m) calculated in Eq. 2 (Berodier and Scrivener 2014).

$$\varphi_m = 1 - 0.45\left(\frac{d_{10}}{d_{95}}\right)^{0.19} \tag{2}$$

$$\delta = \left(\frac{6}{\left(\frac{M_{cement}*BET_{cement}+M_{biochar}*BET_{biochar}}{M_{cement}*BET_{biochar}}\right)\times\rho}\right) \times \left(\left(\frac{\varphi}{\varphi_m}\right)^{\frac{-1}{3}} - 1\right) \tag{3}$$

The average distance between particle centers (H) is calculated by adding the distance between surface of particles (δ) to the weighted average of the average diameter of all particles included in the mix. Using the distance between particle surfaces (δ) found in Eq. 3, and the average distance between particle centers (H) the shear rate experienced by the surface of the particles during mixing (γ) can be modeled by Eq. 4. The speed of the mixer (rpm), the distance from the center of the blade to the edge of the container (R_1) and the radius of the blade (R_2) are all relevant factors in calculating the shear rate on the particles in each mix (Berodier and Scrivener 2014). For this study, rpm, R_1, and R_2 were held constant at 135, 75 mm, and 13 mm, respectively, to maintain consistency in the shear rate induced by mixing between each mix; the mixing bowl geometry did not change since the same mixing equipment was used for each mix.

$$\gamma = \left(2 \times rpm \times 2\pi \times \frac{R_1^2}{R_1^2 - R_2^2}\right) \times \frac{H}{\delta} \tag{4}$$

3.4 Biochar characterization: chemical properties

3.4.1 Proximate analysis

Proximate analysis of the biochars was conducted per ASTM D7582 in duplicate using a LECO TGA and ceramic crucibles (D7582 2015). The volatile matter, fixed carbon content, and ash content were reported as wt.% of the dry biochar (dry basis) to compare all biochars without the influence of variable moisture content.

3.4.2 Ultimate analysis (CHNS/O)

Ultimate analysis was run on each biochar in triplicate to determine the carbon, hydrogen, nitrogen, and sulfur mass percentages. This was performed using a LECO CHN 628 series. Analysis was conducted with a combustion temperature of 950 ℃ and an afterburner temperature of 850 ℃. Organic oxygen content was calculated as: O% = 100%−C%−N%−S%−H%−Ash% to account for the inorganic oxygen and the mass contribution of other inorganic components.

3.4.3 pH

To measure the pH of each biochar, 10 g of biochar was mixed into 100 mL of DI water and stirred at 100–300 rpm on a stir plate for one hour (Singh et al. 2017). Then the biochar was filtered using 3-µm filter paper. A pH probe (Hanna Instruments H2209 pH meter) was immersed into the filtrate and allowed to stabilize before recording.

3.4.4 Ash XRF analysis

To produce ash for elemental analysis, a 10 mL porcelain crucible was filled with biochar and placed in a benchtop muffle furnace at 900 ℃ for at least 24 h, or until the material maintained a constant weight in a TGA program set to heat at 10 ℃ min^{-1} from ambient to 1000 ℃. A vent port in the muffle furnace allowed the ingress of air, enabling the biochar to combust during the thermal treatment. The ashes of each sample were then analyzed for their oxide content using XRF. The Al, Si, Fe, Ca, Mg, S, Na, K, Cl, P, and Ti elements were measured and assumed to be present as simple oxides in the ashed samples. These results were normalized by the wt% ash content of each biochar.

3.5 Data processing methods

To investigate the relevant variables that influence the 28-day compressive strength of biochar cement mortars with a 10% cement replacement, all the measured characteristics were aggregated, and several data processing techniques were applied to analyze variable importance. All data were processed in R with data processing packages: corrplot, dplyr, randomForest, caret, gbm, leaps, and glmnet. With more than 90 predictor variable categories (experimental measurements) and only 16 independent variables (biochar samples), it was infeasible to analyze all possible variable combinations in a best-subset linear model; there would be 2^(# variables) which in this case is 90, resulting in 1.2×10^{27} possible linear combinations. Even if the best-subset was feasible, highly dimensional datasets, such as this one, are susceptible to multicollinearity, meaning there are likely several combinations of biochar characteristic variables that could potentially predict compressive strength results without being mechanistically meaningful.

To better understand the relevant predictor characteristics for compressive strength of biochar cement mortars, Pearson correlations, random forests, and boosted trees (GBM) were employed to study the intercorrelation and importance of individual predictor variables. The ultimate goal of these processing techniques was to optimize the final selection of the most important variables for a multivariate linear model. Principal component analysis (PCA) was used to better visualize the large dataset reduced to 2 dimensions (or principal components). Given the dimensionality of the dataset and the low variability of mortar compressive strength, the multivariate linear model is not recommended for prediction of biochar mortar strength. In the present work, linear modeling was used to help assess the likelihood of proposed hypotheses for improvements to compressive strength and identify biochar characteristics that should be explored further in future research.

3.5.1 Pearson correlation

Pearson correlations provide the strength and direction of correlation between two variables. The closer this score is to 1 or − 1, the more linear the correlation. This technique makes clear which variables are heavily correlated with each other, while also illuminating single variable correlations between a biochar characteristic and the compressive strength. With cross-correlated variables, one must be careful not to use both in a regression model, particularly when one variable can be easily written as a linear combination of the other. Pearson correlations provide insight into variable importance but do not guarantee the best multi-variate linear regression model or consider any data relationships that are not linear.

3.5.2 Random forest and boosted trees

Ensemble methods like decision trees, random forests, and boosted trees are useful machine learning techniques in cases with highly dimensional datasets and output a score for each predictor variable. For the random forest and boosted tree algorithms used, the variable score is the measure of the reduction of Gini impurity that the variable contributes to the model (James et al. 2013). For the random forest model hyperparameters for the number of trees and "m" (the number of predictors to consider at each split) were tuned with tenfold cross validation. Using tenfold cross validation increased the accuracy of the model by training the algorithm on 90% of the data and then testing on the remaining 10%, iteratively. In a similar fashion, a GBM model was constructed with hyperparameter tuning for the number of trees and learning rate "lambda". The random forest model provided higher statistical scores, so the top 40 random forest variables were used as the new variable subset to build linear models. Using the best hyperparameters, the average cross-validation root-mean-square error (RMSE) was 4.32. Unfortunately, the best hyperparameters also resulted in a model that limited the number of variables to be considered for variable importance measures. Therefore, slightly different hyperparameters were used (RMSE of 4.79) that would allow for variable importance measures for nearly all variables across the ten folds. The average cross-validation RMSE for GBM was 6.04.

3.5.3 Linear models with best random forest subset

The top 40 variable scores from random forest were used to build linear models to fit the compressive strength results. Random forest analysis helped reduce the possible linear combinations from 1.2×10^{27} down to 1.1×10^{12}, reducing computational demand. A ten-fold

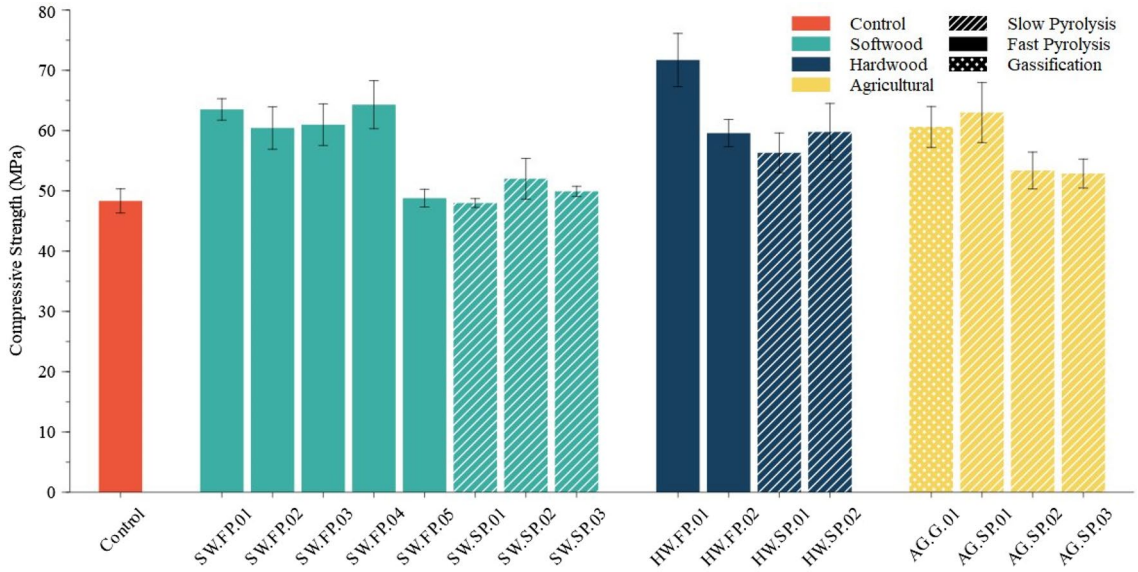

Fig. 5 Unconfined compressive strength of the biochar cement mortars after limewater curing for 28 days. Error bars indicate standard deviation of the triplicate samples tested

cross validation exhaustive best subset model and forward best subset model looped through all variable combinations to determine the top 1 to 11 variables, each time returning the best subset for each fold. After 4 to 5 predictor variables, depending on random seed for the model, the error (RMSE) increased drastically, indicating high variance due to model overfit. The most common variables picked for the best subset across the various folds were then used to create individual multiple regression models with weighted variable equations, RMSE, correlation coefficients, and p-values.

3.5.4 Principal component analysis

With so many predictors and few observations, it was difficult to visualize all the data in any meaningful way. PCA provided a means to reduce the dimensionality of the data to visualize samples in two dimensions by transforming the data to two variables (called principal components). Each principal component comprises all the dataset variables weighted by variance magnitudes. The final outcomes show how each variable drives the variance of the dataset across various principal components as well as which biochar samples are similar.

4 Results

4.1 Compressive strength

Compressive strength was used as the performance metric to evaluate how variance in biochar properties affects the hydrated cement structure. Compared to the control mortar, all the 16 biochar mortar samples had comparable or improved compressive strength after 28 days of limewater curing, as shown in Fig. 5.

A 10% replacement of cement powder with milled biochar exhibited comparable or improved compressive strength after 28 days of curing, regardless of feedstock type or pyrolysis conditions for this subset. However, some biochars increased strength more than others. Most notably, HW.FP.01 improved the control compressive strength by just over 48%.

Table 6 Surface area and average pore size for each biochar sample after milling

Biochar sample	CO_2 surface area [m^2g^{-1}]	Average pore size [Å]	CO_2 pore volume [$cm^3\ g^{-1}$]
SW.FP.01	271.05	13.776	0.0938
SW.FP.02	190.68	13.192	0.0632
SW.FP.03	191.94	13.263	0.0638
SW.FP.04	201.50	12.848	0.0656
SW.FP.05	56.31	13.355	0.0189
SW.SP.01	241.22	13.057	0.0786
SW.SP.02	67.54	14.058	0.0237
SW.SP.03	297.56	13.704	0.1025
HW.FP.01	164.84	13.503	0.0570
HW.FP.02	176.21	13.774	0.0609
HW.SP.01	151.25	13.574	0.0516
HW.SP.02	148.29	13.182	0.0490
AG.G.01	177.20	13.992	0.0623
AG.SP.01	146.27	13.336	0.0491
AG.SP.02	218.52	13.897	0.0764
AG.SP.03	213.80	13.403	0.0719

While both feedstock and pyrolysis process are important predictors of biochar characteristics, it is the physical and chemical characteristics of biochar that directly affect mortar strength development. These final compressive strengths were used as response variables to track which biochar characteristics best correlate with increased compressive strength.

4.2 Physical characteristics

4.2.1 CO_2 surface area and average pore size

The surface area measurements were conducted after milling, which can increase surface area, leading to biochars with relatively high surface area, regardless of feedstock or pyrolysis conditions.

In relation to other characteristics, biochars with higher ash content, and thus a lower carbon content, had decreased surface area. Table 6 summarizes the surface area and average pore size of the micropores, measured on the desorption portion of the BET isotherm hysteresis. The microporosity of biochar comes from the water vapor and volatile matter loss during the pyrolysis process in combination with the feedstock's original pore structure. Consistently, the average pore size of the milled biochar is 13–14 Å.

Surface area plays an important role for nucleation and growth in cementitious systems, with increased surface area providing increased opportunity for nucleation of hydration products (Berodier and Scrivener 2014). However, there is no correlation between surface area and compressive strength ($R^2 = 0.03$), indicating that this characteristic does not have a strong influence on compressive strength.

Table 7 Particle size values for lower limit (d10), median particle size (d50), and upper limit (d95)

Sample	D10 [μm]	D50 [μm]	D95 [μm]
OPC Type I/II	4.38	15.29	41.60
Ottawa Sand	240.00	396.00	581.00
SW.FP.01	4.24	11.00	20.23
SW.FP.02	4.26	12.37	26.95
SW.FP.03	4.10	11.10	22.10
SW.FP.04	4.21	11.84	24.56
SW.FP.05	3.57	8.81	17.13
SW.SP.01	3.57	9.60	17.63
SW.SP.02	2.60	8.24	18.74
SW.SP.03	2.77	7.38	16.25
HW.FP.01	2.87	8.70	21.88
HW.FP.02	4.12	13.53	49.83
HW.SP.01	4.31	11.67	25.87
HW.SP.02	4.00	10.85	22.45
AG.G.01	5.16	13.71	22.16
AG.SP.01	4.14	8.24	17.57
AG.SP.02	3.29	8.01	15.57
AG.SP.03	3.83	8.73	17.08

4.2.2 Particle size distribution

It is critical to mill the biochar to an average particle size of 10–20 μm to eliminate the fragility caused by its

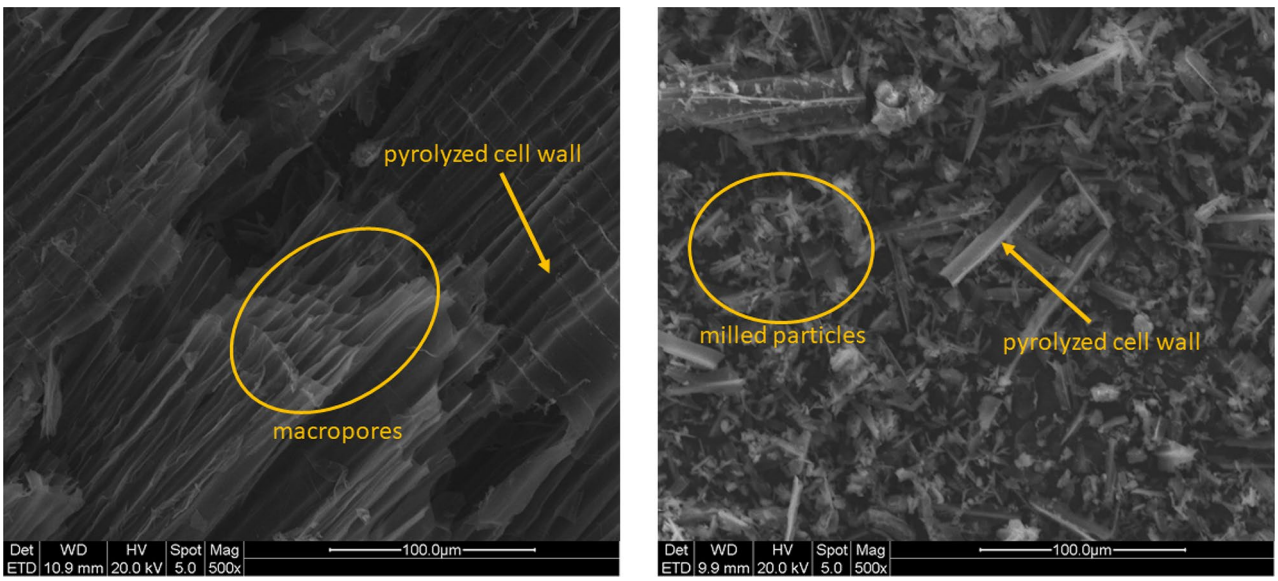

Fig. 6 SEM images of woody biochar produced with slow pyrolysis before (left) and after (right) disc milling showing the reduction of the particle size to eliminate the microporous structure of the feedstock

Table 8 Liquid sorption capacities of biochar samples

Biochar sample	Initial moisture [%]	DI water uptake capacity [%]	Cement pore solution uptake capacity [%]	Initial saturation [%]
SW.FP.01	1.2	109.1	111.9	1.1
SW.FP.02	2.8	100.8	93.6	2.7
SW.FP.03	1.5	106.3	100.9	1.4
SW.FP.04	2.6	93.5	99.9	2.7
SW.FP.05	2.8	102.7	116.7	2.6
SW.SP.01	3.2	71.6	73.4	4.2
SW.SP.02	5.0	66.2	59.2	7.0
SW.SP.03	3.7	89.7	80.6	4.0
HW.FP.01	1.7	118.4	112.1	1.4
HW.FP.02	2.9	127.4	114.8	2.3
HW.SP.01	2.1	96.4	156.0	2.2
HW.SP.02	1.4	96.9	112.8	1.4
AG.G.01	6.3	100.1	106.6	5.9
AG.SP.01	5.7	70.2	104.7	7.5
AG.SP.02	13.4	67.7	101.4	16.5
AG.SP.03	13.7	76.8	79.8	15.1

macropores (Pecha et al. 2022). After exposure to the same milling process, the particle size distributions of each biochar samples were comparable. Consistently, the effective lower limit of particle size (d10) fell between 2.5 and 5 µm and the effective upper limit of particle size (d95) fell between 15 and 30 µm with one exception of the biochar sample HW.FP.02, which had a maximum particle size of ~ 50 µm. Because biochar is weak along the macropores, a short exposure to milling consistently reduces the biochar to an average particle size (d50) of 10–15 µm. Figure 6 shows SEM images of HW.SP.01 before and after milling. Table 7 summarizes the particle size distribution of each milled biochar sample, the OPC, and the sand. All biochars had an average particle size, d50, below both the cement powder and sand.

While no single-variable correlations were found between biochar particle size and mortar compressive strength, since all the milled biochars attained a similar particle size distribution there was likely not enough variation in the biochar particle sizes to account for variability in compressive strength. However, in previous work we have demonstrated that incorporation of unmilled biochar reduces mortar strength by nearly 50% (Pecha et al. 2022).

4.2.3 Liquid adsorption capacity

The liquid adsorption capacity of biochar is an important characteristic for evaluating the hypothesis that biochar improves mortar strength via an internal curing mechanism. The maximum liquid adsorption capacity was measured for each biochar type with both DI water and a simulated cement pore solution. Interestingly, some biochars have higher capacity for DI water than for the pore solution while others show the opposite trend. Table 8 reports the DI water and simulated cement pore solution maximum sorption capacity for each biochar sample, per weight of dry biochar. Fast pyrolysis softwood biochars had higher adsorption capacity than the slow pyrolysis softwood biochars for both liquids. Generally, the sorption capacity for all softwood biochars was comparable regardless of liquid. The hardwood biochars produced by fast pyrolysis had higher DI water sorption capacity than the softwood biochars produced by slow pyrolysis. For all agricultural biochars, the cement pore solution sorption capacity was higher than the DI water sorption capacity, most significantly for the slow pyrolysis biochars.

Interestingly, surface area did not have any linear relationship to the liquid uptake capacity of each biochar, indicating that water sorption is not purely a physical phenomenon in biochars. This suggests that if internal curing is driving strength development in biochar concrete, there is a chemical component that leads to water uptake.

Initial saturation is a metric used to represent how "full" the biochar is with initial moisture compared to its total uptake capacity. Each biochar has a different maximum sorption capacity, so the initial saturation allows for comparison of the liquid uptake potential of the biochars.

DI water was used for the initial saturation calculation rather than the simulated cement pore solution due to the

Table 9 Concentration of ions soluble in DI water for each biochar sample

Sample	Al^{3+} [mg L^{-1}]	Ca^{2+} [mg L^{-1}]	K^{+} [mg L^{-1}]	Mg^{2+} [mg L^{-1}]	Na^{+} [mg L^{-1}]	P^{2-} [mg L^{-1}]	S^{2-} [mg L^{-1}]	Si [mg L^{-1}]
SW.FP.01	0.3	2.8	42.5	1.3	3.6	1.4	1.8	1.2
SW.FP.02	0.6	5.0	39.9	0.6	6.3	0.3	4.2	1.2
SW.FP.03	0.4	5.0	38.0	0.7	2.5	1.1	2.4	1.5
SW.FP.04	0.4	5.0	30.7	0.6	2.0	1.7	2.4	1.6
SW.FP.05	0.2	8.8	44.7	4.0	0.9	2.8	3.4	2.1
SW.SP.01	0.1	6.3	70.3	5.9	1.2	1.5	1.0	1.7
SW.SP.02	0.4	14.2	140.4	0.9	6.1	0.0	42.4	18.4
SW.SP.03	0.5	2.5	42.3	0.9	29.4	1.6	1.4	1.6
HW.FP.01	0.1	5.0	29.0	1.0	2.0	0.4	0.5	4.7
HW.FP.02	0.4	5.8	92.0	1.9	7.6	2.8	4.2	2.7
HW.SP.01	0.2	55.9	65.7	9.5	2.1	118.3	3.4	1.0
HW.SP.02	1.5	16.9	27.7	0.9	4.0	0.0	1.0	6.8
AG.G.01	0.2	6.7	224.7	6.7	5.6	30.1	9.4	2.3
AG.SP.01	0.0	1.1	23.7	1.5	0.7	9.9	0.3	25.2
AG.SP.02	0.0	2.4	57.9	0.7	0.8	0.7	0.3	1.1
AG.SP.03	0.2	3.3	16.6	0.8	50.1	1.8	0.7	1.2

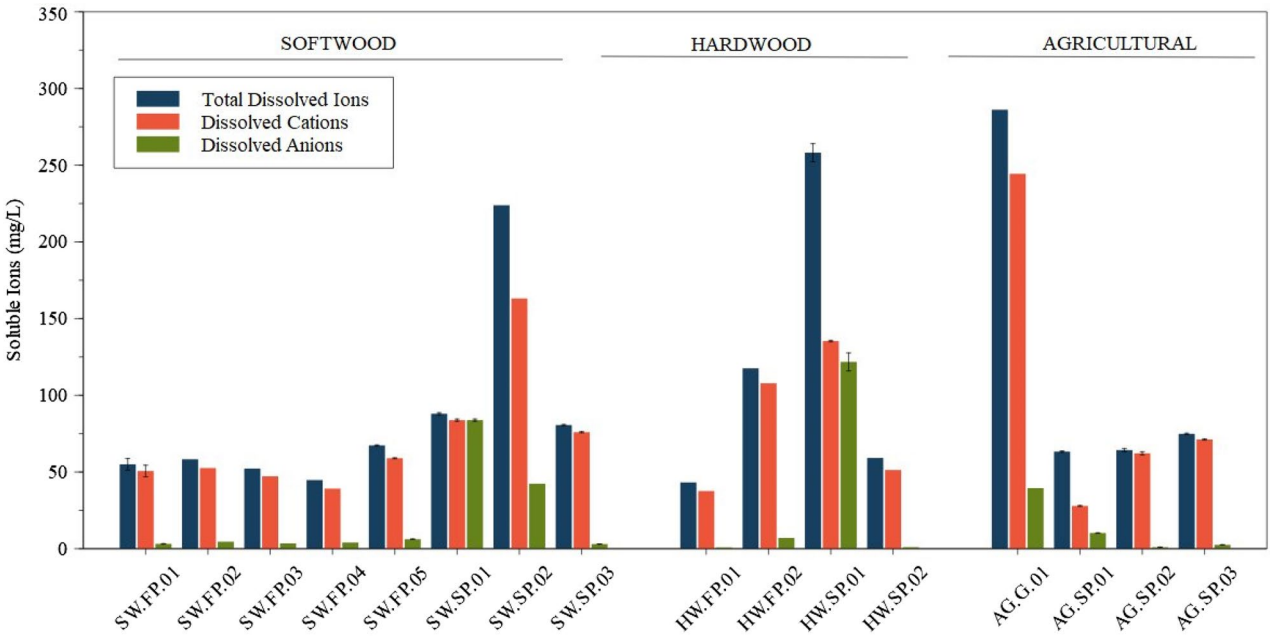

Fig. 7 Concentration (mg L^{-1}) of soluble cations and anions from 1 g of biochar in 100 mL of DI water for 18 h. Remaining charge balance is assumed to be oxyanions not detectable via ICP-AES. Error bars indicate standard deviation of samples run in triplicate

high cation exchange capacity of biochar in pore solution. The exchanged ions cloud the change in mass from pure water uptake. In the future, it may be more prudent to model cement pore solution uptake using a high pH solution that does not contain calcium ions, since the biochar consumes calcium ions while releasing potassium and other cations (shown in Table 10). More work needs to be done to understand the ion exchange between biochar and highly alkaline cement pore solution.

Table 10 Concentration of soluble ions in simulated cement pore solution for each biochar sample

Sample	Ca^{2+} [mg L^{-1}]	K^{+} [mg L^{-1}]	Na^{+} [mg L^{-1}]	S^{2-} [mgL^{-1}]	Si [mg L^{-1}]
Simulated cement pore Solution	437.3	6175.5	2190.5	3149.9	0
SW.FP.01	− 75.2	118.6	29.3	2.3	1.6
SW.FP.02	− 19.3	107.7	84.2	213.5	0.5
SW.FP.03	− 18.6	100.2	83.3	228.3	0.0
SW.FP.04	− 64.5	− 86.0	− 9.6	130.8	1.9
SW.FP.05	− 183.9	− 120.5	− 50.9	44.5	1.1
SW.SP.01	− 146.7	− 300.5	− 127.4	− 79.2	1.6
SW.SP.02	− 201.0	180.8	19.7	115.5	2.3
SW.SP.03	− 116.0	− 224.7	− 55.8	19.6	1.5
HW.FP.01	− 78.4	99.3	7.4	20.8	0.1
HW.FP.02	− 25.2	127.1	69.7	200.6	0.0
HW.SP.01	− 100.6	− 19.5	− 43.8	20.0	0.5
HW.SP.02	− 87.6	131.5	21.1	20.0	0.6
AG.G.01	− 84.6	308.9	25.2	190.6	0.8
AG.SP.01	− 397.4	− 414.2	− 128.1	68.5	23.5
AG.SP.02	116.1	133.2	73.3	298.1	0.0
AG.SP.03	122.7	124.4	− 20.6	155.2	0.0

4.2.4 DI water wash

The leachate from both the biochar-DI-water mixture and the biochar-simulated-cement-pore-solution mixture was analyzed with ICP-AES to determine the concentrations of ions dissolved. Table 9 and Fig. 7 summarize the relevant concentrations of soluble ions for each biochar sample. Though DI water will interact with the biochar differently compared with a highly alkaline cement slurry, this test is an indication of how strongly the inorganic content is bound to the surface of each biochar. After filtration, the leachate was assumed to be at ionic equilibrium, meaning that there should be an equal and opposite anionic concentration for the soluble cation content. These are assumed to be oxyanions not detectable by the ICP-AES method used. The composition of the inorganic content, or ash content, of each biochar is mainly dictated by the feedstock source (Ippolito et al. 2020). Neither dissolved cation concentration nor total charge concentration was found to have any correlation with compressive strength development ($R^2 < 0.2$ for both).

Concrete develops its strength through a complex dissolution–precipitation reaction which ultimately forms hydration products in place of anhydrous cement grains. The progressive dissolution of cement powder is driven by the precipitation of hydration products out of the cement solution as the system tries to maintain ionic equilibrium (Taylor 1997). The addition of biochar with soluble ions has the potential to alter the system's ionic equilibrium and thus the chemical reactions occurring during cement hydration. For instance, the addition of magnesium to a cement system can delay setting time whereas monovalent cations like potassium or sodium can accelerate the setting time (Taylor 1997).

The most important cement hydration product is calcium-silicate-hydrate (C-S–H) which builds compressive strength in concrete (Taylor 1997). Adding a siliceous additive into a cement mix is a common way to increase the precipitation of C-S–H, typically yielding a stronger final product via pozzolanic reactions (Taylor 1997). Silica, present in many of the biochar samples studied here, becomes increasingly soluble as pH increases, so it should be noted that DI water with a neutral pH might not properly model the soluble quantity in cement solutions with a pH of 12–13 (Krauskopf 1956).

4.2.5 Simulated cement pore solution wash

Similar to the DI wash, the biochars were exposed to a simulated cement pore solution and the leachate was analyzed with ICP-AES to evaluate the change in ionic concentrations under conditions similar to a hydrating cement. Table 10 shows the original ionic concentrations for the simulated cement pore solution and each biochar's deviance from that solution after exposure. Interestingly, many of the biochars consumed a significant amount of calcium and potassium from the simulated cement pore solution while releasing sulfur and sodium. The filtrates tested are expected to be at charge equilibrium so the cations consumed or released will need to be in solution with a balanced charge of anions.

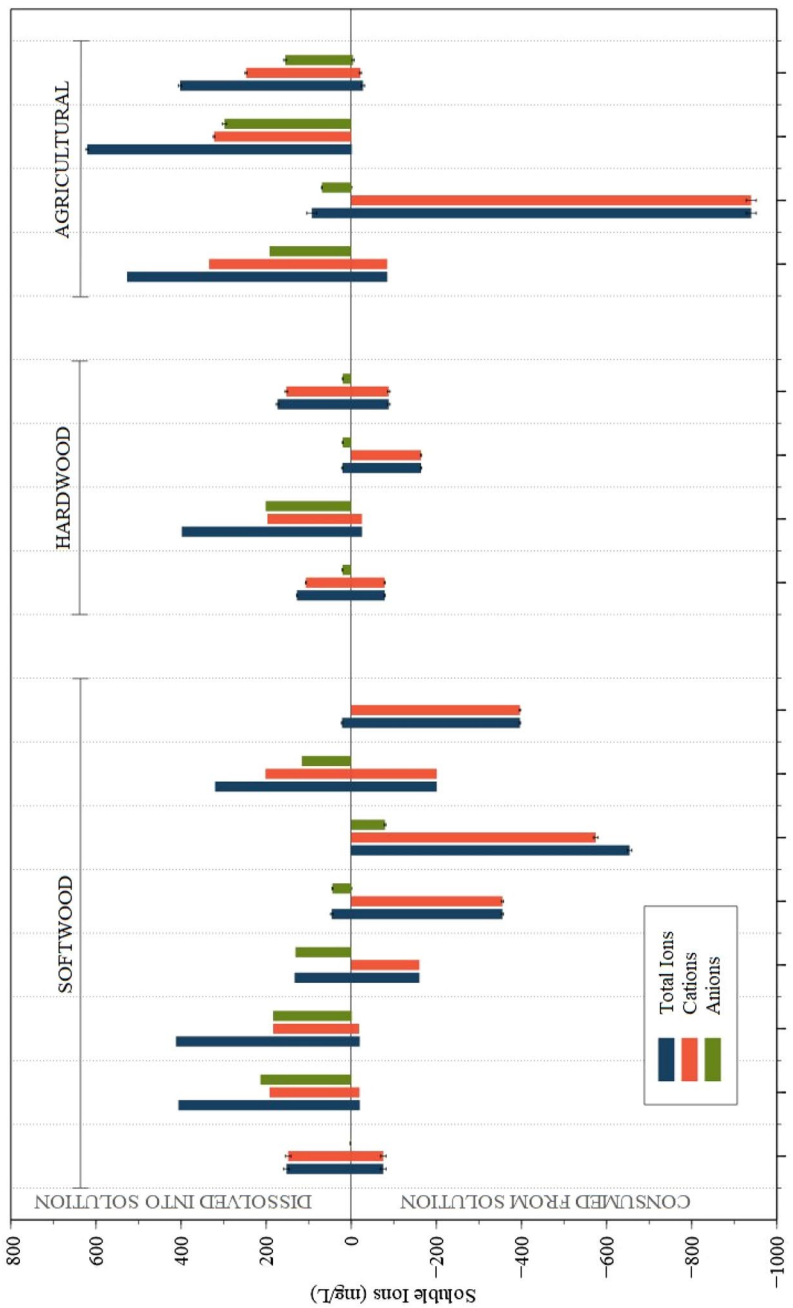

Fig. 8 Concentration (mg L^{-1}) of total ions, cations, and anions soluble in simulated cement pore solution for each biochar sample from 1 g of biochar in 100 mL of simulated cement pore solution for 18 h. Positive concentrations indicate ions that were released into the pore solution. Negative concentrations indicate ions that were consumed from the pore solution. Remaining charge balance is assumed to be oxyanions not detectable via ICP-AES. Error bars indicate standard deviation from triplicate runs

Table 11 Shear rate and interparticle spacing calculation results for each mix design

Sample	$\left(\frac{\varphi}{\varphi_m}\right)$ Relative packing fraction	(δ) Interparticle distance [μm]	(γ) Shear rate [s^{-1}]
Control	0.862	0.1868	1592
SW.FP.01	0.890	0.0094	30,979
SW.FP.02	0.894	0.0155	18,651
SW.FP.03	0.880	0.0165	17,591
SW.FP.04	0.888	0.0168	17,438
SW.FP.05	0.892	0.0127	23,002
SW.SP.01	0.891	0.0138	21,184
SW.SP.02	0.890	0.0130	22,387
SW.SP.03	0.892	0.0120	24,104
HW.FP.01	0.897	0.0097	29,601
HW.FP.02	0.875	0.0359	8230
HW.SP.01	0.877	0.0095	30,884
HW.SP.02	0.896	0.0127	22,999
AG.G.01	0.894	0.0155	18,758
AG.SP.01	0.888	0.0377	7664
AG.SP.02	0.891	0.0105	27,486
AG.SP.03	0.896	0.0102	28,393

These anions could be carbonates, hydroxyls, phosphates, sulfates or other anions. These anions are not detectable with the ICP-AES method used.

This shows that there is more than a purely physical interaction happening when biochar is integrated into cementitious systems, dispelling the idea that biochar is a purely inert filler. This experiment demonstrates biochar's significant cation exchange capacity, shown in Fig. 8. Though there is significant ion exchange occurring in these systems, none of the ion concentrations measured after cement pore solution interaction were statistically significant in predicting final compressive strength.

4.2.6 Shear rate and filler effect

Biochar was added to the cement mortar mix as a fine powder, with an average particle size smaller than the anhydrous cement grains. Biochar is roughly half as dense as cement powder, so a 10% mass replacement results in a much larger volume addition. Adding inert fillers can increase the rate of dissolution of the cement grains in the mix, ultimately increasing the hydration product densification and thus the ultimate compressive strength (Berodier and Scrivener 2014). To investigate the impact of biochar particles on the shear rate of the mix, Eqs. 3 and 4 were used to first calculate relative particle packing and interparticle distance. Using these values, the shear rate was determined for each mix using Eq. 5 (Berodier and Scrivener 2014). Table 11 reports these results. Though all the biochar mixes had significantly lower interparticle spacing and thus a higher interparticle shear rate, none of these factors emerged as highly impactful variables in predicting ultimate compressive strength. All biochar mixes, though, had comparable or increased compressive strength compared to the control, so it is possible that the higher shear rate of biochar mixes contributes some to the strength development of mixes with less cement content. In other words, if not for the increased shear rate compared to the control, it is possible that the biochar

Table 12 Proximate and ultimate analysis of each biochar reported as wt% of the dry mass

Sample	Ash content [wt%]	Volatile matter [wt%]	Fixed carbon [wt%]	Carbon [wt%]	Hydrogen [wt%]	Nitrogen [wt%]	Sulfur [wt%]	Oxygen [wt%]
SW.FP.01	5.6	22.8	71.6	84.4	1.2	0.5	0.0	8.3
SW.FP.02	5.0	26.1	68.9	80.3	3.6	0.4	0.0	19.0
SW.FP.03	4.0	20.7	75.2	81.3	3.4	0.4	0.0	9.6
SW.FP.04	5.5	23.9	70.7	82.8	3.4	0.4	0.0	7.1
SW.FP.05	20.6	48.1	31.4	50.8	3.6	0.4	0.1	10.7
SW.SP.01	5.5	23.9	70.7	43.7	0.6	0.2	0.0	13.7
SW.SP.02	76.6	19.9	3.5	12.1	0.8	0.1	0.4	10.9
SW.SP.03	5.9	18.1	76.0	49.0	3.0	0.3	0.0	7.9
HW.FP.01	8.9	22.5	68.5	78.4	2.7	0.4	0.1	49.9
HW.FP.02	4.2	16.3	79.5	78.4	3.3	0.4	0.0	10.0
HW.SP.01	5.5	34.6	59.9	71.6	3.1	0.7	0.0	41.9
HW.SP.02	15.7	12.5	71.8	76.0	0.5	0.7	0.0	19.8
AG.G.01	3.4	17.3	84.9	42.2	2.2	1.0	0.1	9.0
AG.SP.01	45.7	17.8	36.4	50.8	3.6	0.4	0.1	24.6
AG.SP.02	4.2	5.0	90.8	90.3	1.1	1.0	0.0	3.4
AG.SP.03	4.6	7.2	88.2	89.6	1.3	0.7	0.0	3.8

mortars could have had decreased strength compared to the control. Nevertheless, shear rate was not found to be a good predictor of strength between biochar mixes.

4.3 Chemical characteristics

4.3.1 Proximate and ultimate analysis

Proximate and ultimate analysis are routinely performed on biochar to characterize its chemical composition. Table 12 shows the results of Proximate and ultimate analyses for all biochars used in this study, with all categories reported as wt% of the dried biochar. The carbon content (C%) measured from ultimate analysis includes some hydrocarbons that are present as volatile matter whereas fixed carbon is measured after the volatile matter is removed. Fixed carbon is measured after heating the biochar to 950 ℃, which is above the pyrolysis temperature for many of the samples used, so there is a period of additional depolymerization of carbon prior to the fixed carbon measurement. This is why the C% measured by ultimate analysis is often higher than the value for fixed carbon.

Figure 9 shows a visual representation of the ultimate analysis results for each biochar. Fast pyrolysis biochar typically exhibits a higher carbon content, making its carbon sequestration potential higher. One common way to interpret ultimate analysis is to calculate atomic ratios of the elemental components within a sample in relation to the carbon content. The H/C ratio is used to model the stability of the biochar or the degree of aromaticity; the O/C ratio demonstrates the degree of carbonization and the abundance of oxygen-containing functional groups; and the N/C ratio is used to model the abundance of nitrogen-containing functional groups (Ma et al. 2016).

There is a fundamental correlation between ash content and carbon content for all biochars; the percentage of organic content increases as the inorganic content decreases. Similarly, as carbon content increases, so does surface area, since the inorganic ash is less porous than the carbon structures. C% and O% were found to have a statistically significant relationship with compressive strength ($p=0.08$ and $R^2=0.46$ for C% and $p=0.02$ and $R^2=-0.56$ for O%); though a relatively weak single variable correlation, the statistical significance indicates that these are important variables to consider.

4.3.2 pH

The strength of cementitious composites is primarily attributed to the cement hydration product C-S–H. This forms as part of a dissolution–precipitation reaction, whereby the anhydrous cement dissolves and the ions recombine with water molecules to form hydration products. However, the pH of the cement pore solution can affect both the dissolution of the anhydrous cement particles and the stability of precipitated hydration products. For this reason, the soluble pH of each biochar in DI water was measured, since acidic biochars could alter the hydration kinetics and stability of cement systems. While all the biochars used in this study had alkaline

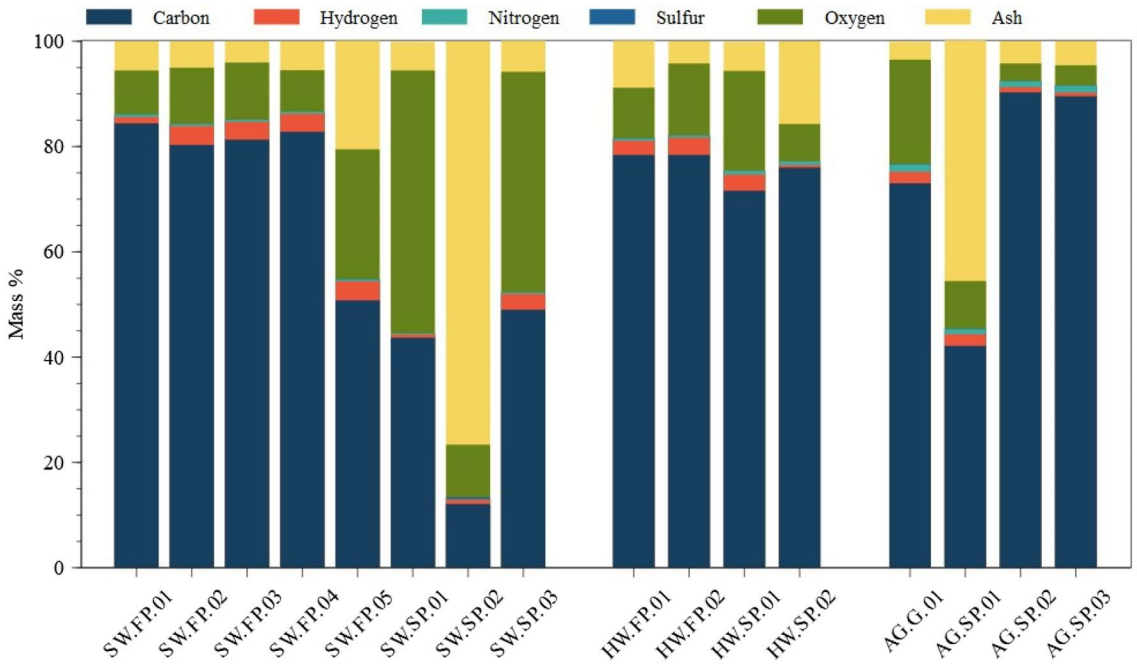

Fig. 9 Ultimate analysis of each biochar segmented by feedstock

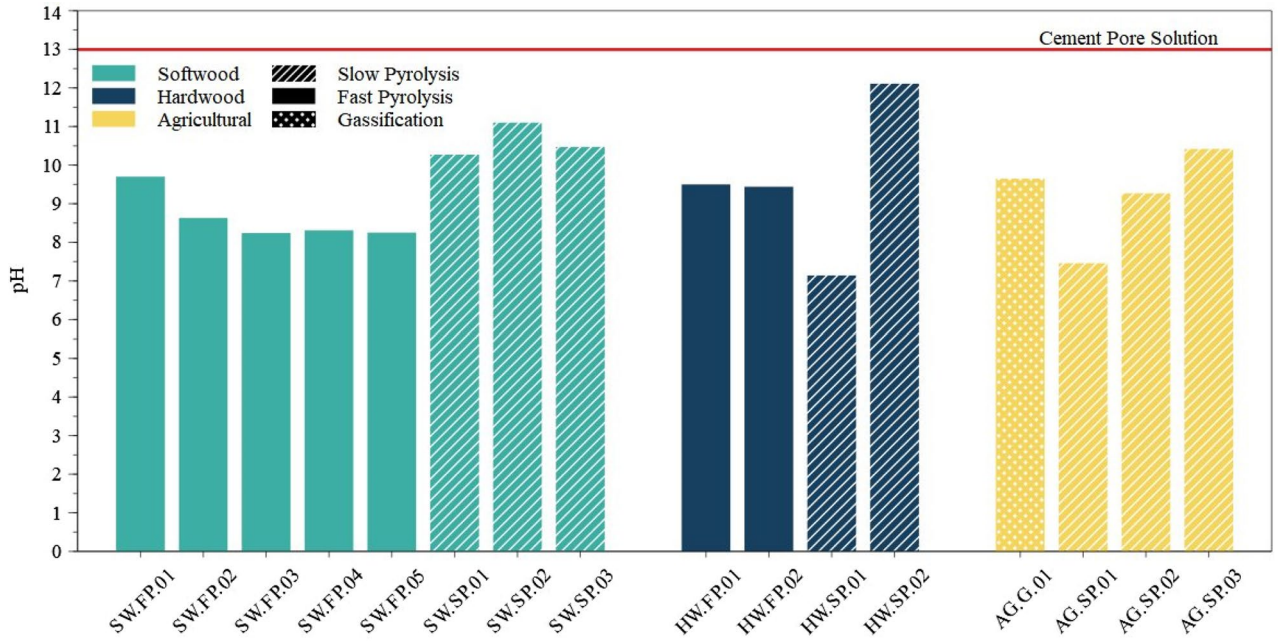

Fig. 10 pH of biochar samples, segmented by feedstock. The red line indicates the pH of the simulated cement pore solution

pHs, shown in Fig. 10, none were as alkaline as cement pore solution which has a pH ~ 13. In general, there was a trend that biochars pyrolyzed at a higher temperature had higher pH. There was a very weakly negative correlation ($R^2 = -0.24$) single-variable correlation between biochar pH and compressive strength, showing that the alkalinity of the biochars had little impact on the strength development.

4.3.3 XRF oxide content

For most of the biochars used in this study, the inorganic ash content is less than 10% of the total biochar mass. Only biochars SW.FP.04, SW.SP.02, HW.SP.02, and AG.SP.01 have more than 10 wt% inorganic content. Total ash content (wt%) is largely driven by feedstock type, and to a smaller degree pyrolysis technique, whereas composition of the inorganic oxides is feedstock specific. XRF cannot detect carbon or oxygen (or any element with less than two valence shells, *i.e.*, any element before sodium in the periodic table) so the XRF results only show the composition of the inorganic components. Though XRF reports elemental compositions, for inorganic ash these elements are assumed to be present as simple oxides. Table 13 shows the composition of each biochar's ash. These values indicate the wt% of oxides normalized by the ash content and the overall dry weight of the biochar. Figure 11 shows the CaO, SiO_2, Al_2O_3, and Fe_2O_3 content in the ash for each biochar, since these can contribute pozzolanic properties in cementitious systems (Taylor 1997).

There was no statistically significant single-variable correlation between any of the measured oxides and compressive strength, likely because most of the biochars had less than 10 wt% inorganic as content and it was not found to be significantly soluble or reactive.

4.4 Statistical data analysis

Principal Component Analysis (PCA) was conducted on the entire set of characteristic variables to condense the dimensionality of this dataset to see what variables and biochar samples are driving variances. Figure 12 shows the first and second principal components of the biochar samples which explain 30% and 18% of the variance in the dataset, respectively. The farther from (0,0) a biochar is plotted on the 2D PCA graph, the more that biochar varies from the rest, considering all measured characteristics. Figure 12 demonstrates that much of the variance within the entire dataset is driven by AG.SP.02, AG.SP.03, SW.SP.02, and SW.FP.05.

The 40 biochar characteristics/variables with the highest variable importance scores were collected and systematically combined in 1, 2, 3, and 4 variable linear models. Each linear model used a tenfold analysis method which trained the algorithm with a randomly selected 90% of the data for each included variable and

Table 13 XRF results for each biochar reported as simple oxides and wt% of total dry biochar

Sample/mix	SiO_2 [wt%]	Al_2O_3 [wt%]	Fe_2O_3 [wt%]	CaO [wt%]	MgO [wt%]	SO_3 [wt%]	Na_2O [wt%]	K_2O [wt%]	P_2O_5 [wt%]	TiO_2 [wt%]
SW.FP.01	1.75	0.44	0.33	1.50	0.34	0.05	0.09	0.68	0.00	0.25
SW.FP.02	1.61	0.48	0.20	1.26	0.50	0.03	0.06	0.43	0.00	0.25
SW.FP.03	1.20	0.26	0.14	1.21	0.40	0.03	0.06	0.31	0.00	0.31
SW.FP.04	2.21	0.28	0.22	1.25	0.45	0.03	0.07	0.53	0.00	0.33
SW.FP.05	11.68	2.47	0.11	4.33	0.46	0.00	0.16	0.92	0.00	0.17
SW.SP.01	0.71	0.21	0.30	2.13	0.97	0.06	0.06	0.23	0.00	0.43
SW.SP.02	40.33	9.61	2.22	13.47	2.45	0.28	0.50	4.67	0.01	1.43
SW.SP.03	1.39	0.44	0.28	1.95	0.45	0.05	0.40	0.49	0.00	0.22
HW.FP.01	4.25	0.11	0.21	2.83	0.38	0.03	0.02	0.69	0.00	0.22
HW.FP.02	1.16	0.20	0.12	1.36	0.43	0.03	0.08	0.38	0.00	0.37
HW.SP.01	0.11	0.02	0.02	1.64	0.30	0.05	0.04	0.84	0.00	2.43
HW.SP.02	7.34	1.19	1.42	3.69	0.49	0.08	0.16	0.87	0.00	0.20
AG.G.01	0.51	0.06	0.10	0.43	0.06	0.17	0.05	0.57	0.00	0.23
AG.SP.01	43.84	0.08	0.11	0.14	0.23	0.00	0.11	0.35	0.00	0.32
AG.SP.02	0.05	0.02	0.04	1.41	0.01	0.04	0.03	1.62	0.02	0.19
AG.SP.03	0.29	0.03	0.07	1.92	0.23	0.11	0.49	0.28	0.03	0.21

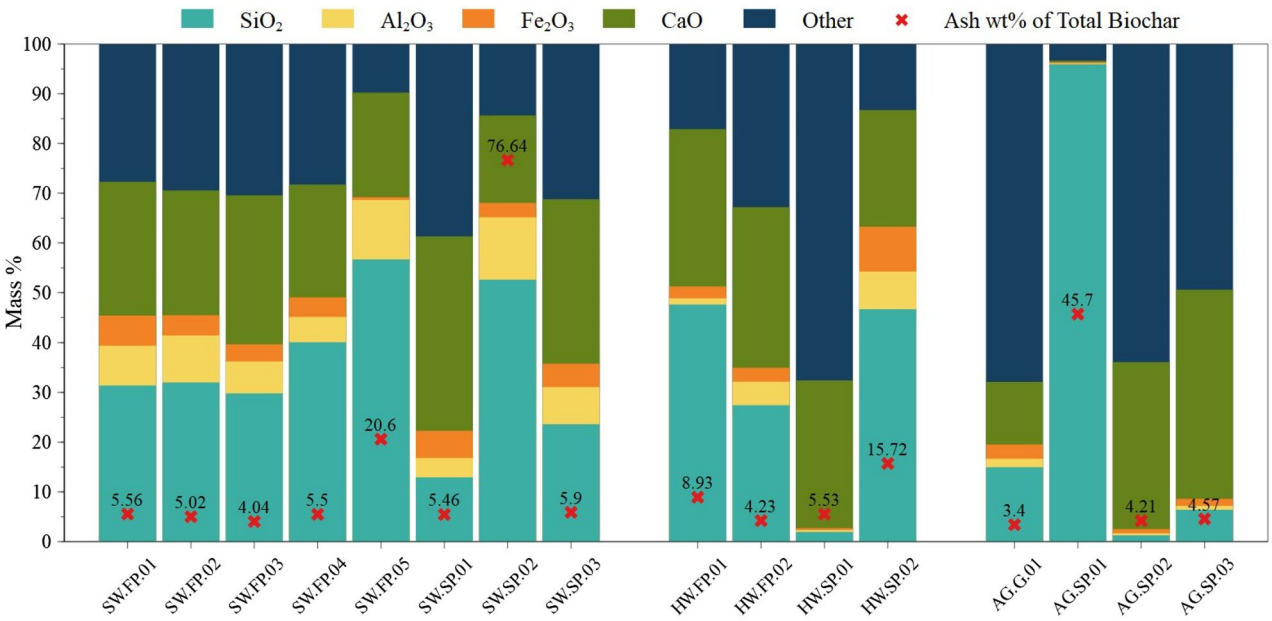

Fig. 11 XRF oxides relevant for pozzolanic activity reported as wt% of total ash content. Red X refers to the total wt% of ash content for each biochar

then validated with the remaining 10%, iteratively. One variable combination emerged as a strong linear model for the compressive strength results: oxygen to carbon atomic ratio, initial saturation %, and soluble silicon wt%. This linear combination, shown in Eq. 5, had an average RMSE of 3.2 MPa, average variance across the 10 folds of 7.3 MPa, and an adjusted R^2 value of 0.71. Figure 13 shows a graphical correlation between the measured compressive strength values for each 10% biochar mortar and the strength calculated from Eq. 5 taking these three key characteristic variables into consideration: initial saturation % (S), silicon content soluble in DI water (Si), and the atomic ratio of oxygen to carbon (O/C). For the linear model, each variable included in Eq. 5 had a statistically significant p-value < 0.05.

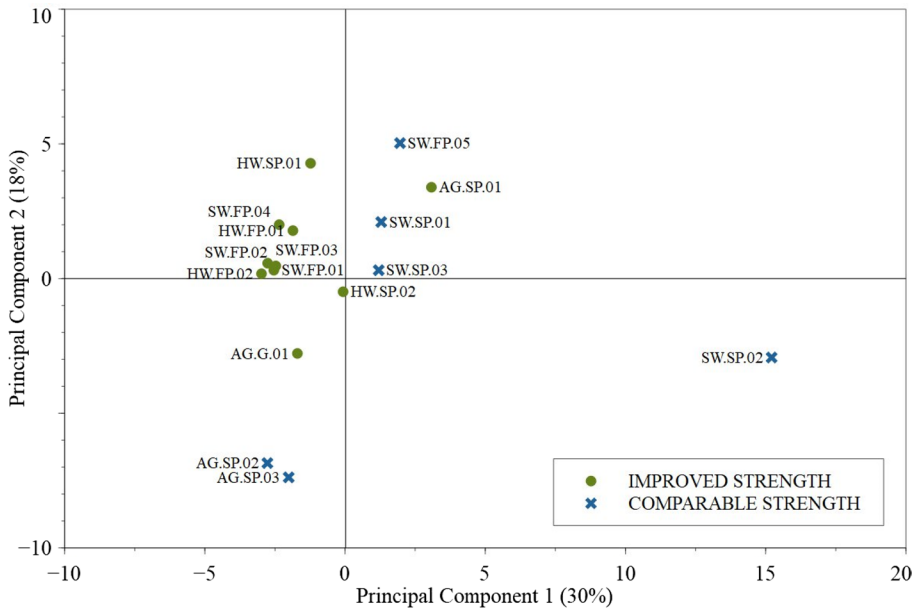

Fig. 12 Scores plot for principal components 1 and 2 showing the variance in biochar considering all measured characteristics

$$10\%\ Biochar\ Compressive\ Strength = 65.03 - 71.2 * S + 0.2 * Si - 18.4 * \left(\frac{O}{C}\right) \quad (5)$$

While this variable combination models this dataset well, it does not mean that another variable combination does not exist that would yield a statistically significant model of these compressive strength results. However, by using additional analysis methods to determine variable importance (random forest and GBM) and reduce the dimensionality of the initial characterization dataset, these limitations can be minimized to produce a strong analysis of the factors impacting compressive strength in this biochar dataset. Confidence in the compressive strength predictor model would also be improved if the biochar-cement mortars analyzed had more variable compressive strength. However, a recent meta-analysis of 51 publications using biochar in cementitious composites also shows a negative relationship between O/C and compressive strength and a positive relationship between Si and compressive strength (Zhao et al. 2024), suggesting that the present analysis is strong despite the dimensionality of the dataset and relatively low variance in observed strength. Unfortunately, most other studies do not characterize the initial saturation percentage of the biochar they use, so it is impossible to assess this model for other datasets reported in literature.

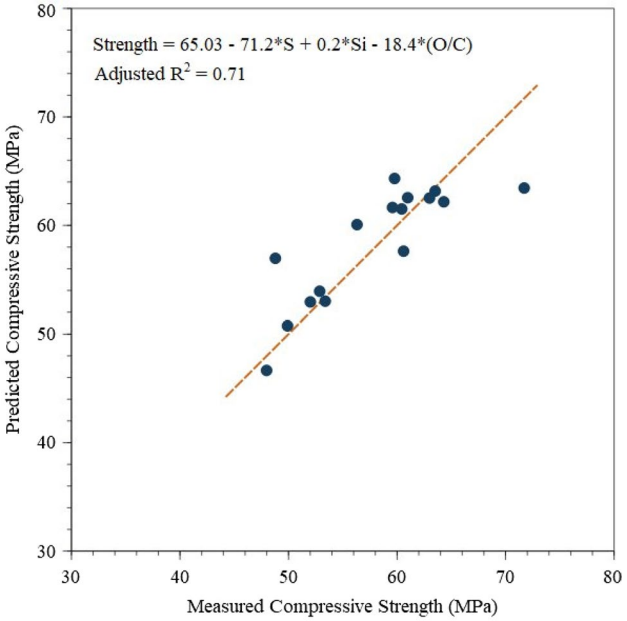

Fig. 13 Comparison of measured compressive strength and predicted compressive strength

5 Discussion

After reducing the set of physical and chemical characteristic measurements with random forest and GBM models, a promising linear regression model was constructed to correlate a combination of biochar characteristics to 28-day compressive strength. This model found that a linear combination of initial saturation %, oxygen to carbon atomic ratio, and the quantity of Si soluble in DI water can explain 71% of the variance in the compressive strength results (adjusted $R^2 = 0.71$ with an RMSE of 3.25 MPa). Figure 13 shows this linear regression model's prediction of 28-day compressive strength compared to measured values for all the biochars in this dataset. The linear regression model shows a negative correlation between initial saturation and compressive strength, a negative correlation between O/C and compressive strength, and a positive correlation between the concentration of soluble Si and compressive strength. The impact of each predictor variable in Eq. 5 is discussed further in the following sections.

These results complement the existing "internal curing hypothesis" with an important distinction. The internal curing hypothesis proposes that biochar's high surface area results in a high sorption capacity, which leads to adsorption of the mix water immediately following integration into a concrete mix and then slow release of that water during the curing period due to a humidity gradient (Bentz and Weiss 2011; Gupta and Kua 2018). This results in a densified cement matrix which improves compressive strength. Since the surface area of biochar was not found to be a statistically significant variable controlling compressive strength, the present work partially supports this mechanism but points to a chemical driver rather than a physical driver controlled by surface area (Kua and Tan 2023; Qing et al. 2023; Suarez-riera et al. 2024). The explanation for this is further developed in Sect. 5.1.

The "filler effect" hypothesis is also dependent on biochar's surface area, as increased filler surface facilitates increased nucleation of hydration products. The impact of a filler effect phenomenon was modeled by calculating interparticle spacing and shear rate. This work does not explicitly disprove the presence of some filler effect occurring, but the variance in interparticle spacing and shear rate experienced by the particles during mixing does not have any significant correlation with compressive strength between biochar types. However, compared to the control mix, all of the biochar mixes had a significantly decreased interparticle spacing and increased shear rate; this could explain why biochar mixes attain comparable compressive strength to the control with 10% less cement, but not why some biochars develop more compressive strength than others.

5.1 Initial saturation % (-)

The initial saturation % of each biochar (the ratio of initial moisture content and total water uptake capacity, calculated in Eq. 1) has a negative influence on compressive strength, meaning that the biochars that were more saturated (normalized by their total capacity) before integration into a mortar mix ultimately developed less compressive strength than biochars that were less saturated and had more available liquid uptake capacity. Initial saturation gives an indication of the *available* water uptake capacity of the biochar, which supports the "internal curing" hypothesis proposed by previous researchers in this field (Maljaee et al. 2021; Zhang et al. 2022; Chen et al. 2023; Kamini et al. 2023; Senadheera et al. 2023). The more mix water that a biochar can uptake (by weight) at the moment of integration (viz., the available liquid uptake %), the lower the effective w/c ratio in the composite after the biochar has fully saturated with mix water, and the higher the strength of the final composite. This is because the initial spacing of the anhydrous cement particles, which is controlled by the w/c ratio, is predictive of the void space in the hardened concrete. Additionally, if the biochar releases the adsorbed water over time, it can facilitate the precipitation of more hydration products, further densifying the pore network and increasing compressive strength. In this trial, the same quantity of biochar was added to each mix, and the biochars that had higher initial saturation compared to their total water uptake potential exhibited lower compressive strengths.

Interestingly, the initial saturation % characteristic was found to be a stronger predictor variable for compressive strength than both total sorption capacity ($R^2 = 0.53$) and surface area ($R^2 = 0.03$), which are typically the measured characteristics associated with internal curing phenomena. In fact, no single-variable correlation was found between surface area and compressive strength in the present work. While the dependence on initial saturation % suggests that internal curing may play a role in strength improvements in biochar cementitious composites, the poor correlation between surface area and strength indicate that water uptake may be driven by chemisorption rather than physisorption. More work needs to be done to understand the interactions between cement mix water and functionalized biochar surfaces.

5.2 Soluble Si (+)

The aqueous concentration of silicon ions dissolved from biochar in DI water was found to have a positive influence on mortar compressive strength. The importance of silicon is well documented for cementitious materials (Taylor 1997). For example, supplementary cementitious materials, such as fly ash and slag, are beneficial as partial cement replacements because they contribute soluble silica, which increases the compressive strength of the final composite via pozzolanic reaction; during this reaction, the soluble silica reacts with the calcium hydroxide produced from the cement hydration reaction to produce more C-S–H. Cement mixes with pozzolanic materials tend to gain strength slowly, reaching ultimate strength well beyond 28 days, whereas the biochar mortars did not seem to have any delay in strength development. It is more likely that the easily soluble silicon in the biochar reacts to form C-S–H first rather than in pozzolanic reactions where the slowly dissolving Si reacts with the $Ca(OH)_2$ produced from the initial cement hydration reaction. This phenomenon also explains why the concentration of soluble silica is higher for the biochar-DI water analyte than for the biochar-pore-solution analyte, despite the solubility of silica increasing as pH increases (Krauskopf 1956). Since the simulated cement pore solution contains CaO, the soluble silica can be removed from solution by precipitating C-S–H, leaving a decreased concentration of soluble silica compared to the DI water analyte. Due to the high pH, it is likely that the soluble silica available for precipitation of C-S–H is actually higher for biochar in a cement pore solution than in DI water; thus, the concentration measured after a DI water wash is likely a conservative estimate of the available silica in a cementitious solution (Krauskopf 1956). It is possible that even stronger correlations with compressive strength would be observed if the simulated cement pore wash experiment were repeated with a high pH solution devoid of calcium.

5.3 O/C atomic ratio (-)

The atomic ratio of oxygen to carbon, measured via Ultimate elemental analysis, accounts for the organic oxygen (not the oxygen associated with the inorganic ash) and the carbon content in each biochar. An increase in this ratio has a negative influence on mortar compressive strength for the biochar mortars studied. While not a direct measurement, this value is indicative of the surface functionality and polarity of the biochar (Suliman et al. 2016). Though ultimate analysis is a bulk measurement, the O/C ratio can indicate the density of oxygenated functional groups on the biochar surface (Bakshi et al. 2020). Higher O/C ratios indicate more functional groups, which increase surface reactivity due to oxygen's inherent polarity. Though the O/C was found to be a relevant variable in this study, the overall carbon % was a close second, with a positive correlation between C% and compressive strength. As seen in Fig. 9, after ash and carbon, oxygen is the most prevalent element in all

the biochars studied, indicating that most of the surface functionalization is present as oxygen functional groups.

Although O/C emerged as the statistically relevant variable, it is likely that the impactful property is surface functionalization in general; meaning that less functionalized biochars integrate more successfully than highly functionalized biochars into cement mixes. There are a variety of reasons that increased surface functionalization could negatively impact the development of compressive strength of cement mortars: acidic deprotonation in high pH environments creating water molecules; increased electrostatic interactions between polar surfaces and ions in solution; or potential other reactions that interfere with hydration product development.

There is no strong correlation in this dataset between O/C and initial saturation % ($R^2 = 0.10$) nor total sorption capacity ($R^2 = 0.39$); this indicates that another property is driving initial saturation other than oxygen surface functionalization. Additional research is needed to fully understand the chemical interactions between biochar and cementitious systems, whereas it is clear that biochar should not be classified as an "inert" additive.

The intent of this statistical model is not to definitively predict the strength of any biochar-cementitious composite, but rather to identify key biochar characteristics that require further investigation. While incorporating biochar into the built environment has the potential to substantially reduce global CO_2 emissions, the field is still relatively new. To increase market adoption of biochar in concrete, it is necessary to understand which biochar characteristics should be controlled. This analysis suggests that initial saturation percentage, O/C, and soluble silicon content are the most important characteristics to control; however, given the high variability in biochar characteristics depending on feedstock and pyrolysis conditions, these conclusions should be validated for other biochars. Future research in this field should include characterization of the initial saturation percentage of the biochar used in cementitious composites, which the present work identifies as the most important variable controlling compressive strength.

6 Conclusions

This work evaluated the compressive strength of cement mortars with 10% of the cement mass replaced with 16 distinct biochars. The pyrolysis conditions, feedstocks, physical characteristics, and chemical characteristics were measured and analyzed with iterative statistical methods to model the impact of each characteristic on the final compressive strength. Through characterization of several chemical and physical characteristics of the 16 biochars, a combination of three variables was found to successfully model over 71% of the variance in mortar compressive strength: initial saturation %, oxygen to carbon atomic ratio, and the water-soluble silicon concentration.

After milling each biochar sample to an average particle size of 10–15 μm, this work shows that a wide variation of biochars can be successfully integrated into cement mortars as a 10% replacement of cement powder without reducing (and often improving) the compressive strength of the composite. More often, the composite strength is significantly increased with incorporation of biochar. This replacement level is double the maximum recommended dosage often reported in published studies in this field, highlighting the potential of biochar to significantly offset the carbon footprint of cementitious composites without decreasing strength.

While three variables emerged as the most important predictors of mortar strength, several important biochar characteristics were identified. We recommend that the following properties are routinely measured and reported for biochar-cement composite studies:

(1) Ultimate analysis (Carbon %, Nitrogen %, Sulfur %, Hydrogen %, and Oxygen %)
(2) Initial moisture content
(3) Maximum liquid sorption capacity
(4) DI water soluble ion concentrations

Note, this analysis should be completed after milling the biochar to an average particle size of ~ 10 μm.

This work indicates that a wide range of biochar compositions can be successful at 10% cement replacement levels with biochar, once milled below the biochar's macroporosity. More work is needed to understand the mechanisms that drive the statistical observations in the present work and to verify that the strength-controlling biochar characteristics identified in this study apply to a broad range of biochars. While the strength of the predictive model should not be overstated considering the relatively small dataset, the analysis is useful for identifying variables that may influence compressive strength of cementitious composites and for illuminating potential mechanisms that warrant further exploration. For example, results of the present work suggest several future research directions that may result in improved understanding of strength development in biochar cementitious composites, such as (1) understanding how biochar surface functionalization interferes with strength development; (2) directly assessing the internal curing hypothesis and the role of chemisorption; and (3) directly assessing the importance of initial saturation percentage by incorporating biochar with no initial moisture. By fully understanding how cement mixes are altered by biochar at a

microstructural level, beneficial properties can be controlled to increase biochar dosages in concrete without sacrificing performance, enabling higher offsets of CO_2. This work highlights key biochar characteristics for use in cement applications, which can be modified by tuning pyrolysis parameters. To optimize biochar for use in concrete, producers should maximize the percentage of carbon, decrease surface oxygenation, use feedstocks rich in reactive silica, and minimize biochar's initial saturation percentage. By tuning the favorable biochar characteristics and increasing biochar loading in concrete, biochar offers a high potential pathway to achieve high-strength, carbon neutral concrete.

Supplementary Information

The online version contains supplementary material available at https://doi.org/10.1007/s42773-024-00375-6.

Additional file 1.

Acknowledgements
The authors would like to thank Ensyn, Glanris, Carbo Culture, Mainstream Engineering, Pacific Biochar, Biochar Solutions Inc, VGrid Energy Systems, and Washington State University for providing biochar samples to be included in this study. Some of the work was performed in following core facility, which is a part of Colorado School of Mines' Shared Instrumentation Facility (Electron Microscopy: RRID:SCR_022048).

Author contributions
Julia Hylton: conceptualization, investigation, visualization, writing—original draft preparation. Aaron Hugen: formal analysis, visualization. Steven Rowland: formal analysis. Mike Griffin: resources. Lori Tunstall: conceptualization, writing—review and editing, project administration, funding acquisition. All authors have read and approved the final manuscript.

Funding
This study was funded by National Science Foundation Award #2139035, the Colorado School of Mines Foundation, and the State of Colorado Advanced Industry program (COEDIT).

Data availability
The datasets collected and analyzed during the current study are available from the corresponding author on reasonable request.

Declarations

Competing interests
All authors have no competing interests to disclose.

Author details
[1]Colorado School of Mines, Golden, USA. [2]National Renewable Energy Laboratory, Golden, USA.

Received: 15 March 2024 Revised: 7 August 2024 Accepted: 9 August 2024
Published online: 15 October 2024

References

Aman AMN, Selvarajoo A, Lau TL, Chen WH (2022) Biochar as cement replacement to enhance concrete composite properties: a review. Energies 15:1–20. https://doi.org/10.3390/en15207662

Arowojolu O, Ibrahim A, McDonald A (2023) The effect of including biomass on the rheological and pozzolanic properties of Portland limestone cement- case study. Sustain Struct 3:1–15. https://doi.org/10.54113/j.sust.2023.000024

ASTM C150 (2000) Standard specification for portland cement. ASTM 93:2–6. https://doi.org/10.1520/C0150

ASTM C778 (2000) Standard specification for standard sand. ASTM International 93:2–6. https://doi.org/10.1520/C0778-17.2

ASTM C1437 (2009) Standard test method for flow of hydraulic cement mortar. ASTM International, West Conshohocken, pp 6–7

Bakshi S, Banik C, Laird DA (2020) Estimating the organic oxygen content of biochar. Sci Rep 10:1–12. https://doi.org/10.1038/s41598-020-69798-y

Barbhuiya S, Bhusan B, Kanavaris F (2024) Case studies in construction materials biochar-concrete : a comprehensive review of properties, production and sustainability. Case Stud Constr Mater 20:e02859. https://doi.org/10.1016/j.cscm.2024.e02859

Bentz DP, Weiss WJ (2011) Internal Curing: A 2010 State-of-the- Art Review. Civil Engineering

Berodier E, Scrivener K (2014) Understanding the filler effect on the nucleation and growth of C-S-H. J Am Ceram Soc 97:3764–3773. https://doi.org/10.1111/jace.13177

Busch P, Kendall A, Murphy CW, Miller SA (2022) Literature review on policies to mitigate GHG emissions for cement and concrete. Resour Conserv Recycl 182:106278. https://doi.org/10.1016/j.resconrec.2022.106278

C109 A (2016) Standard test method for compressive strength of hydraulic cement mortars. Annu Book ASTM Stand 04:1–10. https://doi.org/10.1520/C0109

Chemerys V, Baltrėnaitė E (2017) Effect of modification with FeCl 3 and MgCl 2 on adsorption characteristics of woody biochar. In: 10th International Conference on Environmental Engineering, ICEE. 27–28. https://doi.org/10.3846/enviro.2017.012

Chen L, Zhou T, Yang J et al (2023) A review on the roles of biochar incorporated into cementitious materials: mechanisms, application and perspectives. Constr Build Mater 409:134204. https://doi.org/10.1016/j.conbuildmat.2023.134204

D7582 (2015) A standard test methods for proximate analysis of coal and coke by macro thermogravimetric analysis. ASTM International, West Conshohocken. https://doi.org/10.1520/D7582-15

Delaney M, Hawkes J (2011) Carbon Markets Investment Criteria for Biochar Projects

Dixit A, Gupta S, Pang SD, Kua HW (2019) Waste Valorisation using biochar for cement replacement and internal curing in ultra-high performance concrete. J Clean Prod 238:117876. https://doi.org/10.1016/j.jclepro.2019.117876

EPD I (2023) Sika ViscoCrete-2100. Environmental Product Declaration, Stockholm, pp 1–14

Fidel RB, Laird DA, Thompson ML, Lawrinenko M (2017) Characterization and quantification of biochar alkalinity. Chemosphere 167:367–373. https://doi.org/10.1016/j.chemosphere.2016.09.151

Gupta S, Kua HW (2018) Effect of water entrainment by pre-soaked biochar particles on strength and permeability of cement mortar. Constr Build Mater 159:107–125. https://doi.org/10.1016/j.conbuildmat.2017.10.095

Gupta S, Kua HW (2019) Carbonaceous micro-filler for cement: effect of particle size and dosage of biochar on fresh and hardened properties of cement mortar. Sci Total Environ 662:952–962. https://doi.org/10.1016/j.scitotenv.2019.01.269

Igalavithana AD, Mandal S, Niazi NK et al (2017) Advances and future directions of biochar characterization methods and applications. Crit Rev Environ Sci Technol 47:2275–2330. https://doi.org/10.1080/10643389.2017.1421844

Ippolito JA, Cui L, Kammann C et al (2020) Feedstock choice, pyrolysis temperature and type influence biochar characteristics: a comprehensive meta-data analysis review. Biochar 2:421–438. https://doi.org/10.1007/s42773-020-00067-x

James G, Witten D, Hastie T, Tibshirani R (2013) An introduction to statistical learning: with applications in R, 7th edn. Springer, New York

Kamini GP, Tee KF, Gimbun J, Chin SC (2023) Biochar in cementitious material—A review on physical, chemical, mechanical, and durability properties. AIMS Mater Sci 10:405–425. https://doi.org/10.3934/matersci.2023022

Krauskopf KB (1956) Dissolution and precipitation of silica at low temperatures. Geochim Cosmochim Acta 10:1–26. https://doi.org/10.1016/0016-7037(56)90009-6
Kua HW, Tan SMH (2023) Novel typology of accelerated carbonation curing: using dry and pre-soaked biochar to tune carbon capture and mechanical properties of cementitious mortar. Biochar. https://doi.org/10.1007/s42773-023-00234-w
Lin X, Li W, Guo Y et al (2023) Biochar-cement concrete toward decarbonisation and sustainability for construction: characteristic, performance and perspective. J Clean Prod 419:138219. https://doi.org/10.1016/j.jclepro.2023.138219
Liu J, Liu G, Zhang W et al (2022) Application potential analysis of biochar as a carbon capture material in cementitious composites: a review. Constr Build Mater 350:128715. https://doi.org/10.1016/j.conbuildmat.2022.128715
Ma X, Zhou B, Budai A et al (2016) Study of biochar properties by scanning electron microscope—energy dispersive X-ray spectroscopy (SEM-EDX). Commun Soil Sci Plant Anal 47:593–601. https://doi.org/10.1080/00103624.2016.1146742
Maljaee H, Madadi R, Paiva H et al (2021) Incorporation of biochar in cementitious materials: a roadmap of biochar selection. Constr Build Mater 283:122757. https://doi.org/10.1016/j.conbuildmat.2021.122757
Marshall J, Muhlack R, Morton BJ et al (2019) Pyrolysis temperature effects on biochar-water interactions and application for improved water holding capacity in vineyard soils. Soil Syst 3:27. https://doi.org/10.3390/soilsystems3020027
Maziarka P, Wurzer C, Arauzo PJ et al (2021) Do you BET on routine? The reliability of N2 physisorption for the quantitative assessment of biochar's surface area. Chem Eng J 418:129234. https://doi.org/10.1016/j.cej.2021.129234
Mechtcherine V, Snoeck D, Schröfl C et al (2018) Testing superabsorbent polymer (SAP) sorption properties prior to implementation in concrete: results of a RILEM Round-Robin Test. Mater Struct 51:28. https://doi.org/10.1617/s11527-018-1149-4
Murali G, Wong LS (2024) A comprehensive review of biochar-modified concrete: mechanical performance and microstructural insights. Constr Build Mater 425:135986. https://doi.org/10.1016/j.conbuildmat.2024.135986
Nehdi ML, Marani A, Zhang L (2024) Is net-zero feasible: systematic review of cement and concrete decarbonization technologies. Renew Sustain Energy Rev 191:114169. https://doi.org/10.1016/j.rser.2023.114169
Newalkar G, Iisa K, D'Amico AD et al (2014) Effect of temperature, pressure, and residence time on pyrolysis of pine in an entrained flow reactor. Energy Fuels 28:5144–5157. https://doi.org/10.1021/ef5009715
PCA (2021) Portland Cement EPD. Environmental Product Declaration EPD 195:
Pecha MB, Tunstall LE, Hylton J (2022) Cementitious Biochar Compositions and Methods of Making the Same
Qin F, Zhang C, Zeng G et al (2022) Lignocellulosic biomass carbonization for biochar production and characterization of biochar reactivity. Renew Sustain Energy Rev 157:112056. https://doi.org/10.1016/j.rser.2021.112056
Qing L, Zhang H, Zhang Z (2023) Effect of biochar on compressive strength and fracture performance of concrete. J Build Eng 78:107587. https://doi.org/10.1016/j.jobe.2023.107587
Senadheera SS, Gupta S, Kua HW et al (2023) Application of biochar in concrete—A review. Cem Concr Compos 143:102882. https://doi.org/10.1016/j.cemconcomp.2023.105204
Sigmund G, Hüffer T, Hofmann T, Kah M (2017) Biochar total surface area and total pore volume determined by N2 and CO2 physisorption are strongly influenced by degassing temperature. Sci Total Environ 580:770–775. https://doi.org/10.1016/j.scitotenv.2016.12.023
Singh B, Camps-Arbestain M, Lehmann J (2017) Biochar: a guide to analytical methods, 1st edn. CRC Press/Taylor and Francic Group LLC, Milton Park
Suarez-riera D, Lavagna L, Carvajal JF et al (2024) Enhancing cement paste properties with biochar: mechanical and rheological insights. Appl Sci. https://doi.org/10.3390/app14062616
Suliman W, Harsh JB, Abu-Lail NI et al (2016) Modification of biochar surface by air oxidation: role of pyrolysis temperature. Biomass Bioenergy 85:1–11. https://doi.org/10.1016/j.biombioe.2015.11.030
Tan K-H, Wang T-Y, Zhou Z-H, Qin Y-H (2021) Biochar as a partial cement replacement material for developing sustainable concrete: an overview. J Mater Civ Eng 33:03121001. https://doi.org/10.1061/(asce)mt.1943-5533.0003987
Taylor HFW (1997) Cement chemistry, 2nd edn. T. Telford, London
Tomczyk A, Sokołowska Z, Boguta P (2020) Biochar physicochemical properties: pyrolysis temperature and feedstock kind effects. Rev Environ Sci Bio/Tech 19:191–215
Tunstall LE, Scherer GW, Prud'homme RK (2017) Studying AEA interaction in cement systems using tensiometry. Cem Concr Res 92:29–36. https://doi.org/10.1016/j.cemconres.2016.11.005
Usevičiūtė L (2020) Dependence of pyrolysis temperature and lignocellulosic physical-chemical properties of biochar on its wettability. Biomass Convers Biorefin. https://doi.org/10.1007/s13399-020-00711-3
Wang L, Deng J, Yang X et al (2023) Role of biochar toward carbon neutrality. Carbon Res. https://doi.org/10.1007/s44246-023-00035-7
Wright MM, Daugaard DE, Satrio JA, Brown RC (2010) Techno-economic analysis of biomass fast pyrolysis to transportation fuels. Fuel 89:S2–S10. https://doi.org/10.1016/j.fuel.2010.07.029
Zaid O, Alsharari F, Ahmed M (2024) Utilization of engineered biochar as a binder in carbon negative cement-based composites: a review. Constr Build Mater 417:135246. https://doi.org/10.1016/j.conbuildmat.2024.135246
Zhang Y, He M, Wang L et al (2022) Biochar as construction materials for achieving carbon neutrality. Biochar. https://doi.org/10.1007/s42773-022-00182-x
Zhang Q, Feng P, Shen X et al (2023) Utilization of solid wastes to sequestrate carbon dioxide in cement-based materials and methods to improve carbonation degree: a review. J CO2 Util 72:102502. https://doi.org/10.1016/j.jcou.2023.102502
Zhao Z, El NA, Kau J et al (2024) Biochar affects compressive strength of Portland cement composites: a meta—analysis. Biochar. https://doi.org/10.1007/s42773-024-00309-2